NAVAL POSTGRADUATE SCHOOL

MONTEREY, CALIFORNIA

THESIS

IMPACT OF INJECTOR FABRICATION TECHNIQUE ON THE INJECTION AND ATOMIZATION OF JP-10 FOR HIGH-SPEED AERO-PROPULSION SYSTEMS

by

Brendan R. Philbin

September 2021

Thesis Advisor: Christopher M. Brophy
Co-Advisor: Joshua R. Codoni

THIS PAGE INTENTIONALLY LEFT BLANK

REPORT DOCUMENTATION PAGE	*Form Approved OMB No. 0704-0188*

1. AGENCY USE ONLY *(Leave blank)*	**2. REPORT DATE** September 2021	**3. REPORT TYPE AND DATES COVERED** Master's thesis

4. TITLE AND SUBTITLE
IMPACT OF INJECTOR FABRICATION TECHNIQUE ON THE INJECTION AND ATOMIZATION OF JP-10 FOR HIGH-SPEED AERO-PROPULSION SYSTEMS

5. FUNDING NUMBERS

6. AUTHOR(S) Brendan R. Philbin

7. PERFORMING ORGANIZATION NAME(S) AND ADDRESS(ES)
Naval Postgraduate School
Monterey, CA 93943-5000

8. PERFORMING ORGANIZATION REPORT NUMBER

9. SPONSORING / MONITORING AGENCY NAME(S) AND ADDRESS(ES)
N/A

10. SPONSORING / MONITORING AGENCY REPORT NUMBER

11. SUPPLEMENTARY NOTES The views expressed in this thesis are those of the author and do not reflect the official policy or position of the Department of Defense or the U.S. Government.

12a. DISTRIBUTION / AVAILABILITY STATEMENT
Approved for public release. Distribution is unlimited.

12b. DISTRIBUTION CODE
A

13. ABSTRACT (maximum 200 words)

Effective liquid fuel injection on future high-speed aero-propulsion systems is a critical requirement for high performance in volume-limited flight vehicles. The use of emerging manufacturing methods can potentially deliver favorable injection properties while allowing for complex design integration flexibility. The injection properties were characterized for conventional and alternative fabrication methods, including additive manufacturing, laser drilling, electric discharge machining, and platelet techniques. ANSYS Volume of Fluids-Discrete Phase Model simulations modeled the injection and atomization of JP-10 into a simulated engine environment, and the results were compared to experimental images for similar conditions. The experimental setup utilized planar laser-induced fluorescence to visualize the central jet cross-sectional trajectory of each injector type. This work added a dynamic lateral translation method for additional measurement planes across multiple jet orifices. Computer simulations to date have overpredicted the jet penetration characteristics when modeled as a single jet, ignoring geometry details such as port roughness. The influence of neighboring jets appears to increase the perceived air flow blockage and reduce the effective local fuel-air momentum ratios as fuel flow rates increase. This observation results in the requirement to model adjacent fuel jets to better capture the jet penetration and atomization trends.

14. SUBJECT TERMS
liquid fuel, injection, additive manufacturing, modeling, ANSYS Fluent, discrete phase model, volume of fluid

15. NUMBER OF PAGES
67

16. PRICE CODE

17. SECURITY CLASSIFICATION OF REPORT	**18. SECURITY CLASSIFICATION OF THIS PAGE**	**19. SECURITY CLASSIFICATION OF ABSTRACT**	**20. LIMITATION OF ABSTRACT**
Unclassified	Unclassified	Unclassified	UU

NSN 7540-01-280-5500

Standard Form 298 (Rev. 2-89)
Prescribed by ANSI Std. 239-18

THIS PAGE INTENTIONALLY LEFT BLANK

Approved for public release. Distribution is unlimited.

IMPACT OF INJECTOR FABRICATION TECHNIQUE ON THE INJECTION AND ATOMIZATION OF JP-10 FOR HIGH-SPEED AERO-PROPULSION SYSTEMS

Brendan R. Philbin
Ensign, United States Navy
BS, United States Naval Academy, 2020

Submitted in partial fulfillment of the
requirements for the degree of

MASTER OF SCIENCE IN ASTRONAUTICAL ENGINEERING

from the

NAVAL POSTGRADUATE SCHOOL
September 2021

Approved by: Christopher M. Brophy
Advisor

Joshua R. Codoni
Co-Advisor

Garth V. Hobson
Chair, Department of Mechanical and Aerospace Engineering

THIS PAGE INTENTIONALLY LEFT BLANK

ABSTRACT

Effective liquid fuel injection on future high-speed aero-propulsion systems is a critical requirement for high performance in volume-limited flight vehicles. The use of emerging manufacturing methods can potentially deliver favorable injection properties while allowing for complex design integration flexibility. The injection properties were characterized for conventional and alternative fabrication methods, including additive manufacturing, laser drilling, electric discharge machining, and platelet techniques. ANSYS Volume of Fluids-Discrete Phase Model simulations modeled the injection and atomization of JP-10 into a simulated engine environment, and the results were compared to experimental images for similar conditions. The experimental setup utilized planar laser-induced fluorescence to visualize the central jet cross-sectional trajectory of each injector type. This work added a dynamic lateral translation method for additional measurement planes across multiple jet orifices. Computer simulations to date have overpredicted the jet penetration characteristics when modeled as a single jet, ignoring geometry details such as port roughness. The influence of neighboring jets appears to increase the perceived air flow blockage and reduce the effective local fuel-air momentum ratios as fuel flow rates increase. This observation results in the requirement to model adjacent fuel jets to better capture the jet penetration and atomization trends.

THIS PAGE INTENTIONALLY LEFT BLANK

TABLE OF CONTENTS

I. INTRODUCTION....1
A. BACKGROUND....1
B. MOTIVATION....3

II. RESEARCH OBJECTIVES....7

III. EXPERIMENTAL SETUP....9
A. TEST CELL DETAILS....9
1. Air System....9
2. Fuel System....10
3. Laser Setup....11
4. High-Speed Imaging Setup....12
B. FUEL INJECTOR TEST BLOCKS....12
C. VIDEO ANALYSIS....15

IV. COMPUTATIONAL SIMULATION....17
A. SIMULATION ASSUMPTIONS....17
B. GAS-GAS SIMULATIONS....17
C. VOF-DPM SIMULATIONS....18

V. RESULTS AND DISCUSSION....21
A. GAS-GAS SIMULATION RESULTS....21
1. Ethylene Gas Injection at 0.6 g/s....21
2. Ethylene Gas Injection at 0.8 g/s....22
3. Ethylene Gas Injection at 1.0 g/s....23
4. Ethylene Gas Injection at 1.2 g/s....24
5. Curve-Fit Functions....25
B. VOF-DPM SIMULATION RESULTS....26
C. EXPERIMENTAL IMAGING RESULTS....30
D. VOF-DPM COMPARISON TO EXPERIMENTAL IMAGES....32

VI. SUMMARY AND CONCLUSIONS....35

APPENDIX A. INJECTION PLATE IMAGES....37

APPENDIX B. IMAGE ANALYSIS PROGRAM....39

APPENDIX C. EXPERIMENTAL VIDEO IMAGING RESULTS 45

LIST OF REFERENCES 47

INITIAL DISTRIBUTION LIST 49

LIST OF FIGURES

Figure 1. Typical parameters of liquid jet in crossflow. Source: [3].....2

Figure 2. Liquid jet penetration predictions from empirical studies for q=55.8. 5

Figure 3. Potential variations alternative fabrication methods may produce when manufacturing fuel injectors.....6

Figure 4. Overhead view of air delivery to test section.....10

Figure 5. Diagram of laser setup for the excitement of the fuel-dye mixture following injection. 11

Figure 6. A diagram of the camera setup for viewing fuel injection during testing. 12

Figure 7. SolidWorks model of an injection block. 14

Figure 8. Close up images of the injection sites of used injection blocks.....15

Figure 9. Image analysis results of one frame for detection of fuel jet. 16

Figure 10. ANSYS Fluent computational domain setup for a gas-gas simulation.....18

Figure 11. A close-up image of an injection site on an A15 injector block, and the injector shape used to simulate obstructed injection. 19

Figure 12. Mass fraction of ethylene between 0.03 and 1.0 from the results of 0.6 g/s injection. 22

Figure 13. Mass fraction of ethylene between 0.03 and 1.0 from the results of 0.8 g/s injection. 23

Figure 14. Mass fraction of ethylene between 0.03 and 1.0 from the results of 1.0 g/s injection. 24

Figure 15. Mass fraction of ethylene between 0.03 and 1.0 from the results of 1.2 g/s injection. 25

Figure 16. All curve fit functions for the penetration of gaseous ethylene into a crossflow. 26

Figure 17. Liquid injection edge detection results for the 3.3 g/s fuel mass flow rate simulation through a 0.381 mm hole. 27

Figure 18. Liquid injection edge detection results for the 1.7 g/s fuel mass flow rate simulation through a 0.381 mm hole. 28

Figure 19. Liquid injection edge detection results for the crescent injector-shape simulation....29

Figure 20. Penetration comparison between the 1.67 g/s fuel mass flow rate simulation and the crescent-shaped injector simulation 30

Figure 21. Edge detection results for 0.381mm injector hole sizes made with EDM (A) at 52.0 g/s, additive manufacturing (B) at 49.6 g/s, laser drilling (C) at 47.6 g/s, and platelet design (D) at 42.8 g/s.....31

Figure 22. Experimental penetration results for four 0.381mm injector hole sized blocks at similar fuel mass flow rates.....32

Figure 23. Penetration comparison between a 3.33 g/s fuel mass flow simulation and a 3.2 g/s fuel mass flow experimental result. 33

Figure 24. Penetration comparison between a 1.67 g/s fuel mass flow simulation and a 2.2 g/s fuel mass flow experimental result. 34

LIST OF TABLES

Table 1. Summary of test conditions in previous works of liquid injection into a crossflow. Adapted from Marzbali [4]. 4

Table 2. Specifications, dimensions, and manufacturing methods of injector blocks. 13

Table 3. Manufacturing details of the previously used injection blocks. 15

Table 4. Ethylene penetration curve fit functions. 26

THIS PAGE INTENTIONALLY LEFT BLANK

LIST OF ACRONYMS AND ABBREVIATIONS

DPM	Discrete phase model
D_0	Jet diameter
EDM	Electrical discharge machining
FMG	Full Multigrid
PLIF	Planar laser induced fluorescence
q	Fuel/Air momentum flux ratio ($\rho_j v_j^2 / \rho_\infty v_\infty^2$)
U_∞	Freestream velocity
V_j	Jet velocity
VOF	Volume of fluid

THIS PAGE INTENTIONALLY LEFT BLANK

ACKNOWLEDGMENTS

I want to thank Dr. Chris Brophy and Dr. Joshua Codoni for their constant support and guidance during my research. I'd also like to give a special thanks to Alexis Theony for his expertise and excellent instruction regarding ANSYS and its simulation tools, without which this thesis would not have been possible.

THIS PAGE INTENTIONALLY LEFT BLANK

I. INTRODUCTION

A. BACKGROUND

As world powers, territorial claims, and military strengths have grown and changed the international landscape over the past few decades, new air-breathing weapons systems have emerged as fast and effective forms of strike attack and defense that possess significant range capabilities. Within the past few decades, long-range air-breathing missiles that travel between Mach 2 and Mach 4 speeds have become a popular system across the globe due to their platform flexibility, fast response time, and reliability. Most current and historic platforms utilize rocket motors for propulsion that are relatively simple, reliable, and have favorable storage characteristics, but these motors lack significant range due to the requirement to carry both fuels and oxidizers for propellant. Rocket motors have evolved over the past several decades to improve their range capability and remain a popular choice for many missile systems today but still lack the capability to deliver significant payloads over flight distances exceeding 100 miles when constrained to size and mass limitations associated with tactical systems.

The ever-increasing range requirements for tactical missile platforms is the motivation behind utilizing air-breathing propulsion systems with their significantly higher specific impulse and thus increased range. Where rocket motors must carry both fuel and oxidizer components, air-breathing propulsion systems only need to carry fuel onboard and utilize captured air as the oxidizer, which allows for a significant increase in range and stand-off distance. With a much farther range, missiles that utilize air-breathing propulsion systems would be able to perform a time critical strike at greater standoff distances where solid rocket motors could not, allowing for improved naval deterrence. Additionally, air-breathing systems have increased mission flexibility as they can often fly more tailorable trajectories and be re-tasked after their launch, unlike most rocket-propelled systems. Air-breathing systems that hold potential for future use include ramjets, scramjets, high Mach turbines, and even rotating detonation engines. These propulsion systems will be able to accomplish a larger variety of missions as compared to rocket-propelled systems and have recently seen a resurgence in research and development over the past two decades in order

to maintain similar tactical capabilities with adversaries who have also pursued this development path.

Traditional methods of fuel injection in air-breathing propulsion systems utilize splash plate injectors, airblast atomizers, air-assist atomizers, or piezoelectric injectors to atomize and vaporize the fuel before combustion [1]. However, with more novel manufacturing methods and complex propulsion system requirements, new injection approaches and design flexibilities emerge. By tailoring the fuel injection geometry and associated distribution, fuel such as JP-10 can atomize and vaporize following injection into a crossflow simply due to the flow conditions within the system, [2] as depicted in Figure 1. This would eliminate the need for splash plates or other aids that often increase internal flow losses while possibly introducing unique manifold and flow path design requirements.

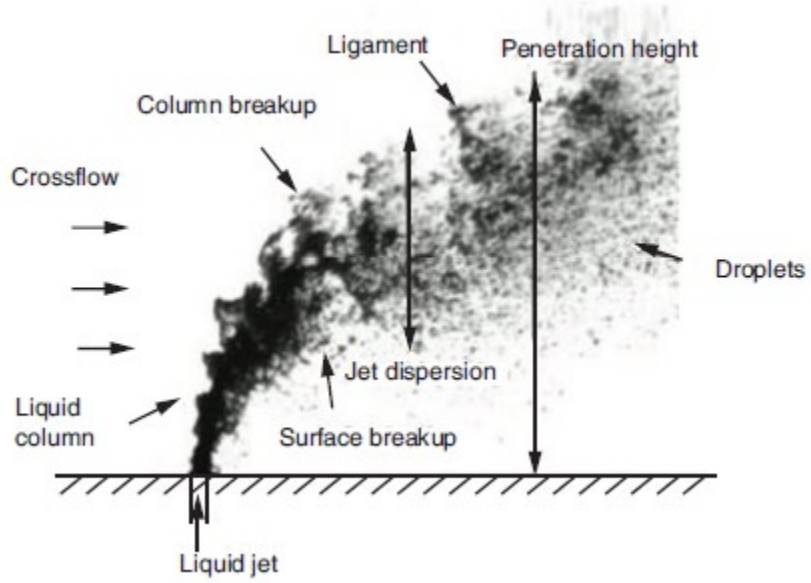

Figure 1. Typical parameters of liquid jet in crossflow. Source: [3].

Manufacturing methods such as laser drilling, platelet technology, electrical discharge manufacturing (EDM), and additive manufacturing allow for fuel manifold and injection geometries that are impossible to create with more traditional manufacturing

processes. These fabrication methods can possibly increase endothermic fuel use and regenerative cooling to be integrated into engine designs to significantly reduce the volume and mass of an engine such that the fuel injection system could be locally tailored to a specific shape to improve thermal management. Ultimately, these production methods may allow for engines to be designed towards a specific airframe and to their unique mission sets while potentially reducing manufacturing costs. If an engine requires a specific fuel-to-air ratio or fuel mass flow globally or locally, the injectors within the engine can be made specifically for that purpose allowing the engine to adapt to the mission instead of the reverse. With the flexibility and freedom of these manufacturing methods, future engines and aircraft can adapt and change to new environments and system requirements effectively and rapidly.

B. MOTIVATION

Liquid injection into a crossflow has been extensively studied in the literature [2]-[10], with many liquids having been tested at a wide range of momentum ratios. Many of the different analysis methods are listed in Table 1. The wide range of research conducted within this field has shown the importance of momentum ratio (q) between the liquid jet and air crossflow as well as the intrinsic properties of the liquid. Even with changing physical properties between various liquids used in experimentation, equations based on empirical data have been formed that can be used to predict liquid jet penetration given a specific momentum ratio [2, 6, 7, 9, 10]. A number of these relationships can be seen compared side-by-side in Figure 2. Other analytical methods also utilize Weber number [8] or measured drag coefficients [2] to determine breakup characteristics; however, relationships that rely solely on momentum ratio can still produce useful and accurate penetration predictions. Despite the research conducted on this topic, limited comparisons between simulation and empirical observations have been completed. Although completing empirical studies has proven very useful, the creation of an analytical tool can greatly reduce the loop between idea, creation, tests, and results and speed up development processes.

Table 1. Summary of test conditions in previous works of liquid injection into a crossflow. Adapted from Marzbali [4].

Author(s)	Liquid type	D_0 (mm)	V_j (m/s)	U_∞ (m/s)	Momentum ratio	Analysis type	Pressure and temperature
Inamura et al. [35]	Water, Aluminum suspension	0.5, 1.0, 2.0	7-26	55-140	2.5- 225	Back-lighted photography	Atmospheric
Wu *et al.* [25], [26]	Water, Ethyl Alcohol, Alcohol/water, Glycerol/water	0.5, 1.0, 2.0	8.9-37.7	68.1-141	3.3-185	Pulsed shadowgraph, PDPA	Atmospheric
Hassa and Becker [27]	Jet- A1	0.45	N/A	50-100	2-18	Shadowgraph, Mie scattering, PDA	Elevated
Tambe [28]	Water, Jet-A1, N-Heptane	0.38, 0.76	3-26	89-215	0.7-10.2	Pulsed shadowgraph, PDPA	Atmospheric
Cavaliere *et al.* [36]	Water, Jet-A1	0.3, 0.5	10-55	20-55	5-280	Numerical model	Elevated
Madabhushi [37]	Water	0.5	12.8-42.5	68.7- 137	9- 48.8	Numerical model	Atmospheric
Ng *et al.* [38]	Water, Ethyl Alcohol	0.5, 1.0, 2.0	7- 50	10-60	9- 1199	Pulsed shadowgraph, high speed imaging	Atmospheric
Stenzler *et al.* [29]	Water, Acetone, 4-Heptanone	0.29	1.3-16.3	10.8-118.7	9, 14, 18	Mie scattering, PDPA	Atmospheric, elevated
Amighi *et al.* [31]	Water	0.4, 0.5	6.8-54	22-156	10-80	Pulsed laser sheet illumination	Atmospheric, elevated
Mashayek *et al.* [32]	Water, Acetone, Ethyl alcohol, Glycerol, etc.	0.45, 0.5	20	75-100	2-72	Theoretical model	Atmospheric, elevated

Traditional studies on the subject of fuel injection into a gaseous crossflow utilized clean and perfectly cylindrical injection channels that agreed well with known theory. However, fuel injectors and injection systems manufactured through alternative methods will not have the same uniformity. Injection port profiles may not be perfectly circular, injection channels may contain varying levels of roughness along the walls, and the entrances to those injection channels may also not be ideally shaped, as seen in Figure 3. As different manufacturing methods produce these imperfections to varying degrees, they could cause internal flow distortions that improve the atomization of the fuel following injection. Additionally, the local flow features between jets in a linear array may

significantly impact the penetration depth achieved by each. A gaseous crossflow that encounters a single jet can easily pass around it, but when that same crossflow encounters a linear array of jets, the jet deflection may become more pronounced due to the perceived blockage increase. These factors may play a minor or significant role in the atomization performance of the fuel jets and may result in the spray to behave differently than what traditional theory would predict for a single fuel jet in crossflow. Utilizing an analytical model allows the isolation of each of these variables and, when compared to empirical results, could expose the significance of each on a fuel injector's performance.

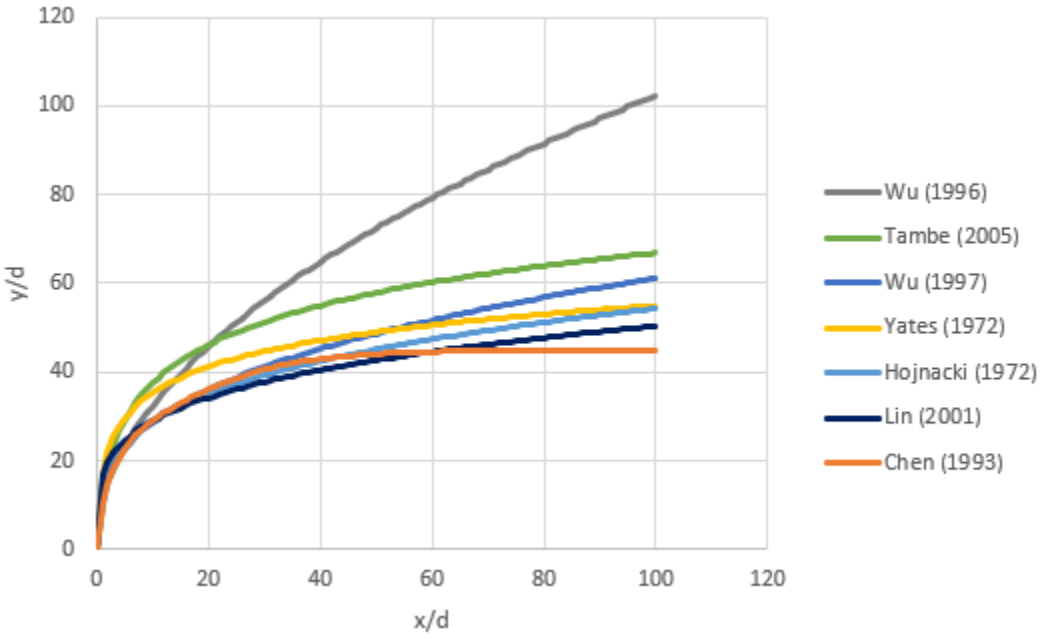

Figure 2. Liquid jet penetration predictions from empirical studies for q=55.8.

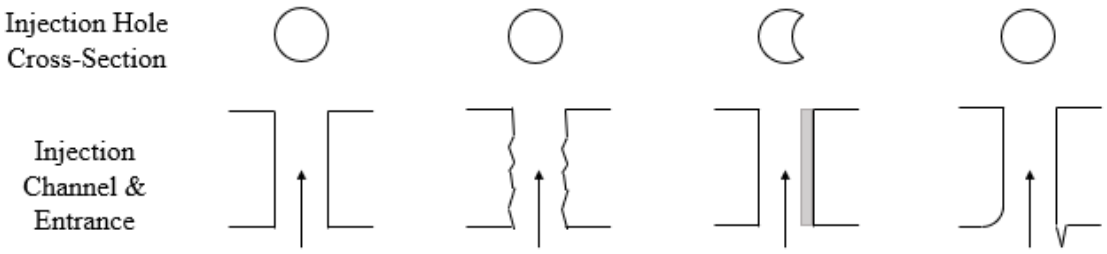

Figure 3. Potential variations alternative fabrication methods may produce when manufacturing fuel injectors.

The impact of the variables discussed above on the delivered fuel injection characteristics needs to be understood for proper design and modeling of fuel injection concepts. The jet-in-crossflow fuel injection approach being considered, with various manufacturing techniques, has the potential to not only reduce total pressure loss, but it can become more tailorable to flight conditions and/or inlet distortion. An analytical model of the jet breakup and atomization dynamics could achieve this while simultaneously improving the research and design process. This model could additionally aid in identifying other factors that influence the penetration and atomization of liquid fuel through the selection of specific assumptions within the model and comparison of those results with empirical data, further improving the ability to tailor propulsion systems to specific conditions.

II. RESEARCH OBJECTIVES

There are three objectives within this thesis that are derived from the ultimate goal of obtaining a validated computational model for liquid jet injection into a crossflow:

- Customize and validate a computational model to study and characterize jet breakup and atomization dynamics with real fuel properties
- Characterize jet penetration as a function of manufacturing technique and momentum ratios
- Develop an image analysis program for experimental images obtained through Planar Laser-Induced Fluorescence (PLIF)

Computational simulations of liquid hydrocarbon sprays have not been performed by staff at the Naval Postgraduate School Rocket Propulsion Lab and hold potential to save significant cost and time when innovating and changing fuel injection methods or techniques. Fuel injection, atomization, and vaporization properties can be tailored by modeling, simulating, and intelligently down-selecting appropriate experimental test components. The first goal allows for future experimentation with theoretical fuel injector designs and could dramatically shorten the design, test, and improve design loop. The second and third goals deliver a foundation for future design and development activities at the Naval Postgraduate School, where fuel injection blocks will be tested and analyzed for their effectiveness at fuel dispersion for potential use in aero-propulsion systems. By creating the tools and methods required to fully analyze and predict fuel injection properties, future work can be expedited, and results can be accelerated and incorporated into future systems.

THIS PAGE INTENTIONALLY LEFT BLANK

III. EXPERIMENTAL SETUP

A. TEST CELL DETAILS

Initial experimentation for this work was performed just as the COVID-19 pandemic began and included the testing of different injection blocks made through various manufacturing methods. The testing was cut short due to the COVID-19 pandemic, and the experimental setup was left untouched for many months but eventually was modified to allow for improved testing and analysis capabilities. The final experimental setup had four main subsystems: the air system, fuel system, laser sheet optical layout, and high-speed imaging setup.

1. Air System

Air was delivered to the test cell from the main air supply system and could be isolated before entering the test cell by a manual ball valve. The air first passed through a choked orifice plate to meter the air mass flow rate delivered to the test cell. Meter air mass flow rates were measured by recording the total pressure and total temperature of the air upstream of the choked orifice and applying an empirically-determined discharge coefficient to the measured area of the choked orifice plate. The air was then directed to a vitiator unit. For the initial work, the vitiator was not utilized. For future work, where matching the desired enthalpy for the fuel injection testing is desired, the vitiator would be operated using hydrogen as a fuel source and ignited by a spark plug. Downstream of the vitiator, the air continues through another flange before it reaches a point where additional oxygen could be added to the air flow to return the oxygen mole fraction to 21%. Both the hydrogen and oxygen flow rates are also controlled by choked orifice plates; however, as previously stated, the vitiator was not utilized during the period of this thesis.

The air piping leaving the vitiator (Location A in Figure 4) was tapped to measure pressure and temperature (Location B). From here, the air is routed through a series of expansion joints and flow-conditioning perforated plates. The air passes through the first expansion joint at the 5.08cm to 7.62cm expansion section (Location C), then proceed through two perforate plates, first at the 7.62cm to 15.24cm expansion flange junction

(Location D), and again at the 15.24cm to 20.32cm expansion section (Location E). The turbulence was increased at each plate, promoting better mixing and preventing separation. The flow conditioning components consisted of two 1.59mm perforated plates with 1mm holes and 50% porosity at each expansion section of the air piping that each expanded the flow into larger diameter piping. The last flange connection before the optical test section (Location F) held a screen with 1mm holes to condition the uniformity of the air one final time before it entered a rectangular cutout of the downstream flange. The final cutout in the last flange measured 19.05cm wide and 3.81cm tall in the center of the flange, which were the same cross-sectional dimensions as the test section. Injection "blocks" could then be inserted flush with the floor of the test section and the resulting injection event could be illuminated through the glass window in the test section ceiling and imaged through the glass windows in the test section walls. Lastly, the air passed through an exhaust tube (Location G) before safely exiting the rig.

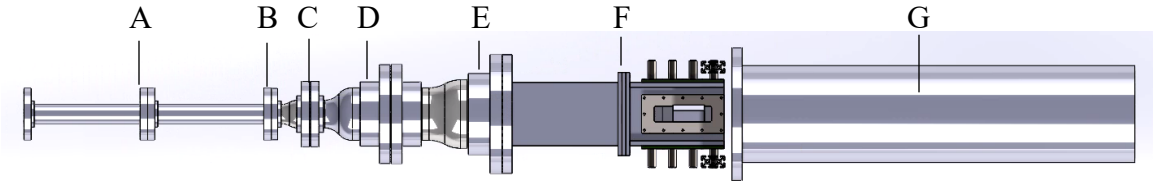

Figure 4. Overhead view of air delivery to test section.

2. Fuel System

The fuel supply pressure was set and delivered by a HYDAC accumulator pressurized with gaseous nitrogen. The liquid JP-10 fuel was mixed with a fluorescent pyrromethene 567 dye before entering the accumulator at a ratio of 1g of dye to 3.78L of fuel so that a uniform mixture can be pumped through the injection block in the test section. The pressure within the accumulator was used to control the mass flow of the fuel into each injector block and was varied to test different flow rates and momentum ratios. Fuel mass flow rates were calibrated during prior experimentation by delivering a set pressure differential to the injector block and measuring the collected mass over a recorded time duration.

3. Laser Setup

The dyed fuel was injected into the test section and excited by a 532 nm laser sheet formed from the output of a Nd:YAG laser. The laser was mounted on a support fixed to the testing table adjacent to the test section and the output beam passed through a lens that spread the beam on one axis which was then reflected by a mirror down into the test section and into the injected fuel spray. Previously, the expansion lens and turning mirror were limited by a small translation stage for fine optical adjustments, which limited overall lateral translation of the laser sheet to study multiple fuel jets. The setup was adjusted for this work to allow for greater lateral translation of the optics and expanded optical measurement capability. To this end, the lens and mirror were suspended from a rail fixed to a linear actuator mounted on a support fixed to the table. The linear actuator allows for a lateral translation of the laser sheet perpendicular to the air flow, and will permit the laser sheet to illuminate any desired plane of the injected fuel. This will allow for future analysis of the effects fuel jets have on each other based on their relative location on the injection block and in the passing air flow. During experimentation, the laser would excite the dye within the fuel and cause it to fluoresce at 575 nm to be captured by the high-speed camera. The entirety of the laser setup was contained within optical beam dumps in order to contain the laser and maintain laser safety. A basic diagram of the laser setup without shielding can be seen in Figure 5.

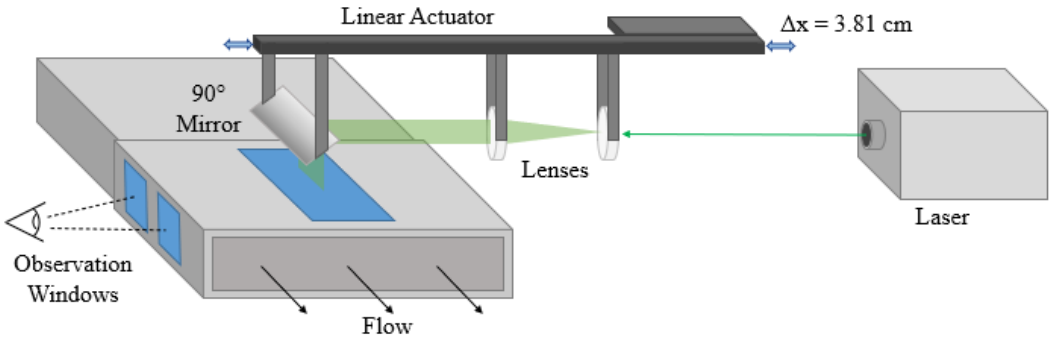

Figure 5. Diagram of laser setup for the excitement of the fuel-dye mixture following injection.

4. High-Speed Imaging Setup

A Photron Fastcam SA-Z was mounted on the opposite side of the test section as the laser setup and was aligned parallel to the air flow. The camera mount was fixed to the table and held the camera lens at the same height as the test section and could image the flow in the test section by observing an image reflected off a 90° mirror. The camera was then able to view the fuel injection site and its penetration into the test section and its downstream breakup. A ruler was placed at the injection site in order to adjust the camera's focus and to be used later as a reference for determining spatial resolution for measuring penetration depth and other length scale characteristics. The camera captured images at 50 kHz with a 575 nm high-pass filter so that it only captured the light emitted from the excited dye. A basic diagram of the camera setup used with a picture from previous experimentation can be seen in Figure 6.

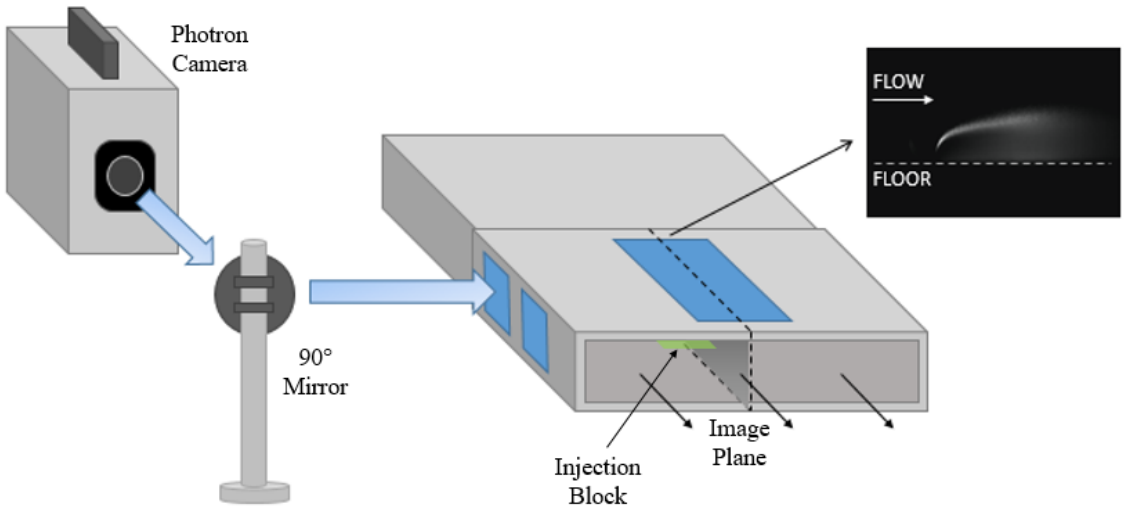

Figure 6. A diagram of the camera setup for viewing fuel injection during testing.

B. FUEL INJECTOR TEST BLOCKS

Fuel injection blocks were manufactured via EDM, platelet technology, additive manufacturing, and laser drilling. Images of all the injector blocks can be seen in Appendix A. An array of injector hole sizes were selected to be manufactured: 0.127 mm (0.0050"),

0.203 mm (0.0080”), 0.304 mm (0.0120”), 0.381 mm (0.0150”), 0.508 mm (0.0200”), 0.635 mm (0.0250”), and 0.762 mm (0.0300”). The injector holes in each block were arranged in a line perpendicular to the direction of the air flow over the block’s surface and had a constant spacing between each injection site. The spacing between holes varied between block diameter sizes, increasing as the injection hole increased in diameter, as described in Table 2. The general shape of all the manufactured injection blocks can be seen in Figure 7, and the injection blocks previously used for testing and the spacing between injection holes can be seen in Figure 8 with the manufacturing details listed in Table 3.

Table 2. Specifications, dimensions, and manufacturing methods of injector blocks.

Design Hole Size [mm]	Fabrication Method				Hole Quantity	Hole Spacing [mm]
0.152	EDM				76	0.67
0.203	EDM	Platelet	Laser		42	1.21
0.305	EDM			AM	19	2.95
0.381	EDM	Platelet	Laser	AM	12	4.56
0.508	EDM		Laser	AM	7	8.44
0.635	EDM				4	17.02
0.762				AM	3	25.47

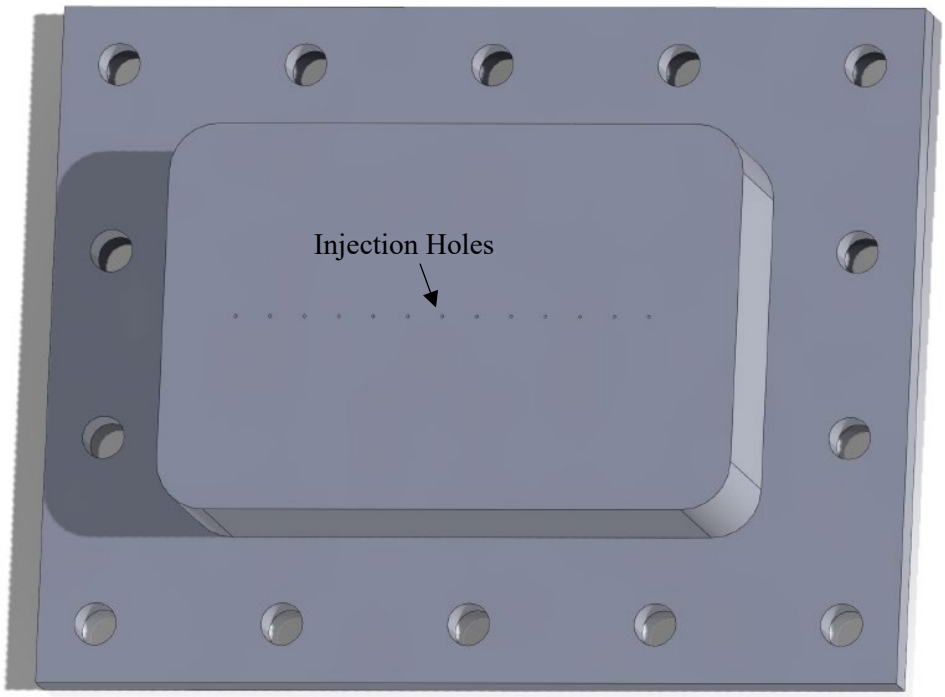

Figure 7. SolidWorks model of an injection block.

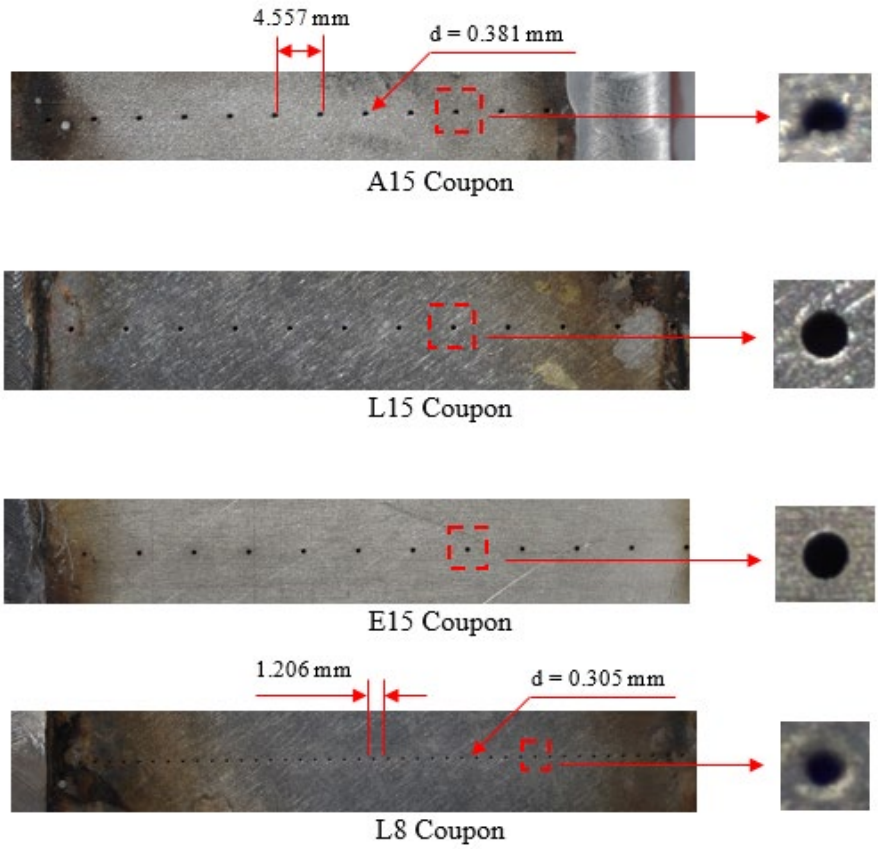

Figure 8. Close up images of the injection sites of used injection blocks.

Table 3. Manufacturing details of the previously used injection blocks.

Injector Label	Manufacturing Method	Design Hole Size [mm]	Hole Spacing [mm]
A15	Additive Manufacturing	0.38	4.56
L15	Laser Drilling	0.38	4.56
E15	EDM	0.38	4.56
P15	Platelet Design	0.38	4.56
L8	Laser Drilling	0.20	1.21

C. VIDEO ANALYSIS

Raw video files were acquired and imported into a MATLAB R2020b script in order to determine the fuel's path and penetration depth and is included in Appendix B. Each test video was viewed in its entirety and a stretch of 300 frames were selected where the fuel was continuously being pumped into the testing section, after the flowfield achieved steady-state operation. This portion of the video was isolated from the rest of the

trial's full video for analysis. A frame was chosen that depicted an average penetration depth for the video clip, brightness values were then normalized for background intensity, and a specific pixel coordinate location was designated to be the location of the injection hole of the injection block illuminated by the laser sheet. Beginning at the column containing the fuel jet origin and for 300 columns downstream, the topmost pixel that contained a luminosity of 5% or 10% above the background was identified and recorded as a point along the edge of the fuel jet. When all of the pixel coordinates are put together for all of the columns, the points then identified the furthest definitive location of fuel for that frame as seen in Figure 9. The data sets for each of these luminosity values were taken into Excel where fourth-order polynomial curve fits could be generated after switching the x- and y-axes for later comparison with analytical results from the computer simulations.

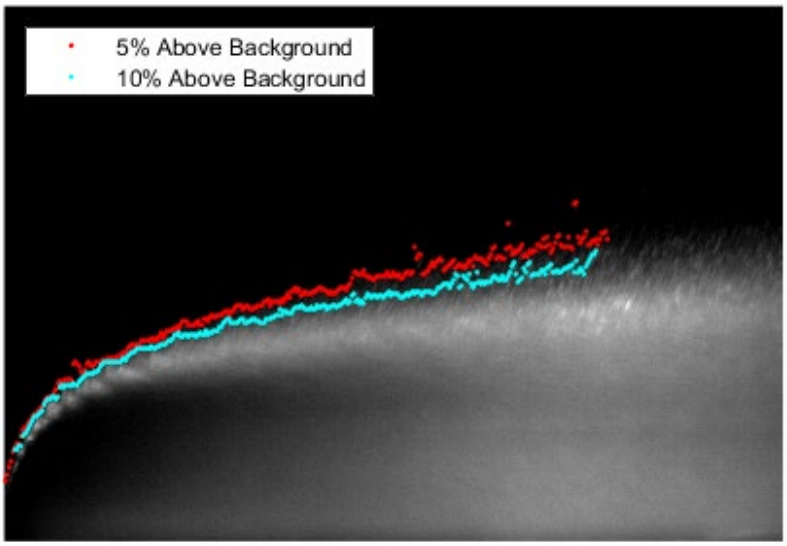

Figure 9. Image analysis results of one frame for detection of fuel jet.

IV. COMPUTATIONAL SIMULATION

A. SIMULATION ASSUMPTIONS

Two variations of ANSYS software were used in this thesis: ANSYS 2020R2 for all-gas fluent simulations and ANSYS 2021R1 for volume of fluid (VOF) and discrete phase modeling (DPM).

The internal volume of the test section for all simulations was assumed to be rectangular and smooth on all sides for ease of recreation in ANSYS SpaceClaim modeling. The fuel injection paths were also assumed to be perfectly cylindrical and originating from a uniform body of fuel, removing most internal turbulence due to wall roughness and local supply flow variations within the fuel manifold of the injector blocks. A k-epsilon turbulence model was assumed for the air flow in the computed volume and utilized the default turbulence properties assigned by Fluent. The fuel velocity profiles in the orifice holes were computed separately with an increased mesh density and subsequently mapped to the boundary condition where the fuel enters the test section for steady-state conditions. The test section geometry was limited to a 2.54 cm wide portion of the original testing section with a single injection site located in the middle. This geometry was further simplified to only have 1.27 cm of upstream space prior to the injection site and 10.16 cm of downstream space, as the fuel injection penetration and atomization results would be able to be properly analyzed given this reduced volume. The air was assumed to be at 300 K with a backpressure of 300,000 Pa which was similar to the conditions from previous experimentation.

B. GAS-GAS SIMULATIONS

In order to establish the feasibility and confidence for two-phase simulations, simulations were first run that contained only gas phases. These simulations used the simplified geometry of the test section with ethylene as the fuel instead of JP-10 and a modified injection orifice hole diameter of 1.524 mm, as seen in Figure 10. The air mass flow was taken from previous experimental data and scaled for the reduced volume being simulated, while the fuel mass flows were varied between 0.6 and 1.0 g/s in order to view

the effect of different momentum ratios on the fuel's injection and dispersion. The ethylene fuel was assumed to be at 400 K in order to avoid the fuel's critical point at higher speeds which could have caused problems within the simulation. For all simulations, hybrid and full multigrid (FMG) initialization methods were used before utilizing a flow Courant number of 5 for the solution, which was set to run for 10000 iterations to establish near steady-state conditions. If any solution variables were changed, first the Courant number would be decreased to 1 or 0.7 to aid in arriving at a solution followed by an increase or decrease in iterations if necessary.

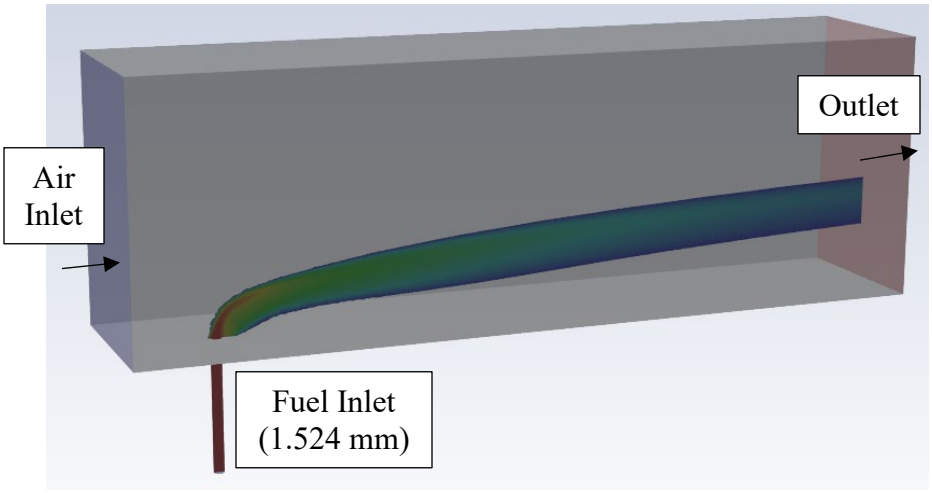

Figure 10. ANSYS Fluent computational domain setup for a gas-gas simulation.

C. VOF-DPM SIMULATIONS

ANSYS 2021R1 was utilized for the VOF-DPM simulations of liquid fuel injection into a crossflow due to its improved simulation capabilities as compared to ANSYS 2020R2. The same test section dimensions were used as in the gaseous simulations to maintain continuity, but the injection orifice was modified to 0.381 mm for the liquid fuel. The simulated liquid was given the same properties as JP-10 in order to best simulate the environment and testing conditions of the previous experimentation.

A single-orifice mass flow rate of 3.33 g/s of the JP-10 liquid was set for the first VOF-DPM simulation to replicate a total mass flow rate of 40 g/s across the 0.381mm hole

size injector blocks, and a second simulation was run at half the mass flow rate (1.67 g/s) to simulate a 20 g/s total fuel mass flow case. The injection hole and channel were set to be circular and perfectly cylindrical to simplify the injection simulation. The passing air was set to achieve 280 kg/s-m^2 with a 4 atm. backpressure in order to replicate engine conditions. The VOF-DPM simulations utilized an adaptive mesh that started with approximate 1 million cells and quickly increased upwards of 100 million cells to accommodate the breakup and atomize in the crossflow.

After observing injector hole obstructions at the surface of the additively manufactured injector blocks, as seen in Figure 11, a third simulation used a crescent-shaped injector hole and channel to evaluate whether the shape would cause noticeable changes to the fuel's behavior following injection and to see if the model reproduced results seen in experimentation. The injection velocity of the fuel was matched to that of the 1.67 g/s fuel flow rate so that fuel behavior following injection could be studied.

Figure 11. A close-up image of an injection site on an A15 injector block, and the injector shape used to simulate obstructed injection.

THIS PAGE INTENTIONALLY LEFT BLANK

V. RESULTS AND DISCUSSION

A. GAS-GAS SIMULATION RESULTS

All gas-gas simulations were able to be run successfully using the parameters mentioned previously, with each taking approximately 8 hours using 256 cores on the Hamming supercomputer at the Naval Postgraduate School. The results were analyzed along a centerline plane of the fuel jet to allow a clear cross-section view of the fuel injection and dispersion downstream. Using this plane, the mass fractions of ethylene was analyzed for comparison between the different fuel injection mass flows for characterization of each. An ethylene mass fraction of 0.03 was chosen for the edge detection characterization of each fuel injection since it is representative of the ignition limits for the ethylene fuel.

1. Ethylene Gas Injection at 0.6 g/s

Due to the low resulting momentum ratio for the 0.6 g/s ethylene flow rate case, the momentum of the air flow dominated the injection event. The results seen in Figure 12 revealed the fuel penetration was limited to about 6 mm above the test section floor. Once the ethylene had been deflected by the crossflow after injection, it traveled with and nearly parallel to the test section floor. Very little dispersion occurred as the ethylene traveled downstream, as seen in the small mass fraction cross-section at x/d=20.

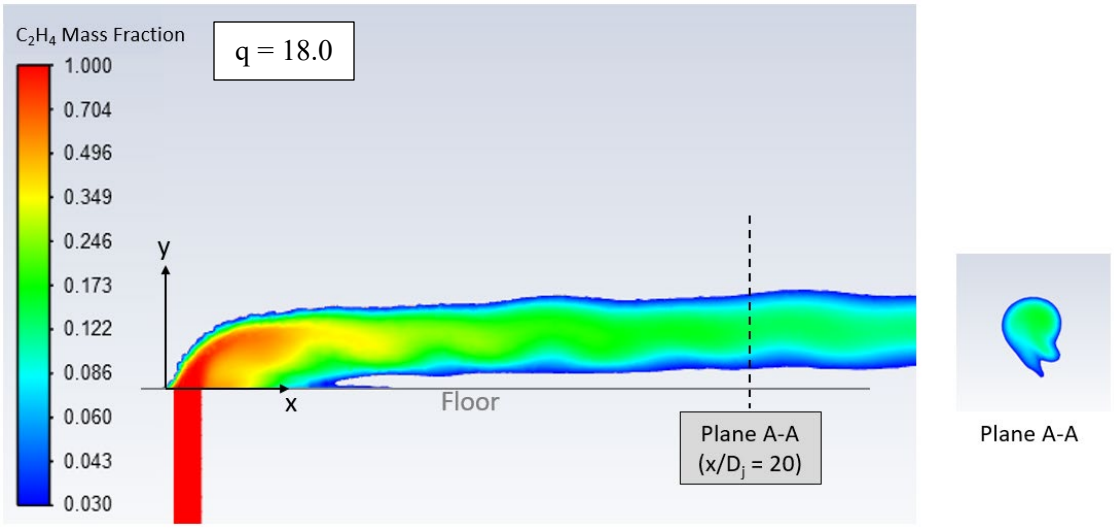

Figure 12. Mass fraction of ethylene between 0.03 and 1.0 from the results of 0.6 g/s injection.

2. Ethylene Gas Injection at 0.8 g/s

Similar to the 0.6 g/s injection case, the crossflow had a significant influence on the ethylene following injection. The results show that the Kelvin-Helmholtz instabilities were seen to have a great effect on the results plane in the 0.8 g/s injection case, as seen in Figure 13. This was due to the ethylene having enough momentum to initially penetrate the crossflow, but as the momentum faded, the ethylene succumbed to growing instabilities and took on a wave-like dispersion. The instabilities caused a large amount of spreading seen in the mass fraction cross-section at x/d=20 due to the "fluttering" nature of the ethylene following injection, which led to significant dispersion further downstream.

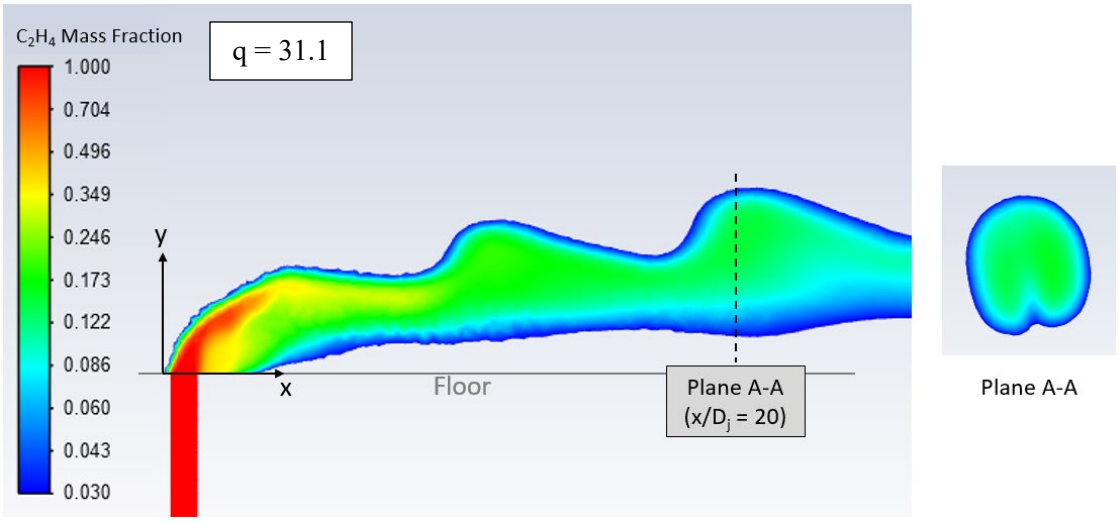

Figure 13. Mass fraction of ethylene between 0.03 and 1.0 from the results of 0.8 g/s injection.

3. Ethylene Gas Injection at 1.0 g/s

The 1.0 g/s injection case was the first case to not witness any evidence of the Kelvin-Helmholtz instabilities. The 1.0 g/s results seen in Figure 14 show that the momentum of the ethylene allowed for steady injection and continued penetration well downstream of injection. The results additionally revealed that near-uniform spreading occurred to the ethylene following its injection, resulting in a very circular mass fraction image at x/d=20. The small disturbance on the bottom side of the cross-section indicates some amount of instability, potentially due to recirculation, likely contributes to ethylene dispersion further downstream.

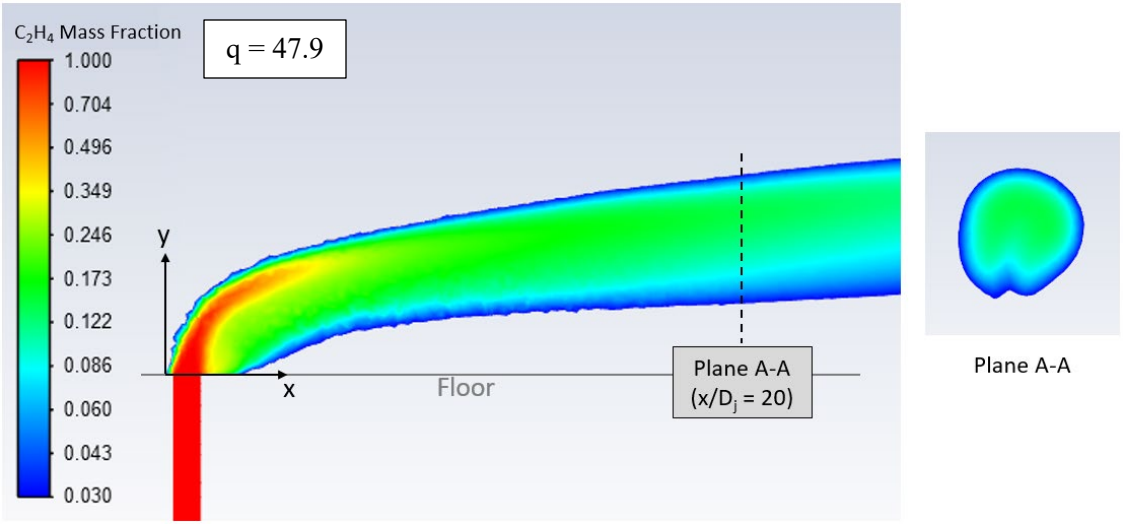

Figure 14. Mass fraction of ethylene between 0.03 and 1.0 from the results of 1.0 g/s injection.

4. Ethylene Gas Injection at 1.2 g/s

As expected, the results of the 1.2 g/s injection case showed that the ethylene penetrated the furthest into the test section and had fair downstream dispersion, as seen in Figure 15. The penetration distance continues to grow well after the ethylene is first injected, just as the 1.0 g/s case did. The mass fraction cross-section at x/d=20 is similar in size to that of the 1.0 g/s injection case but includes protruding tails off the bottom, indicating that further downstream dispersion occurs due to some recirculation behind the ethylene stream.

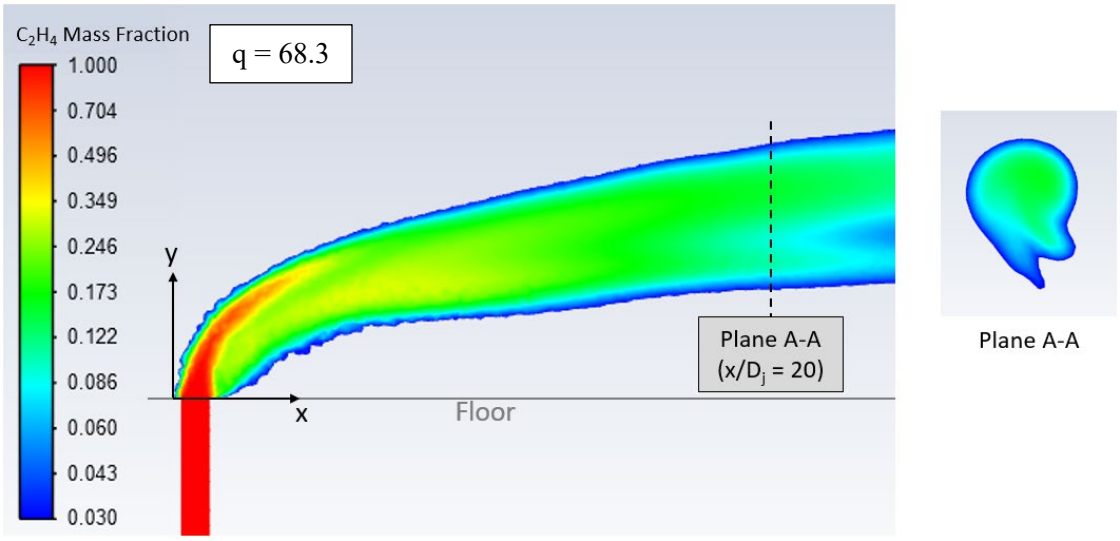

Figure 15. Mass fraction of ethylene between 0.03 and 1.0 from the results of 1.2 g/s injection.

5. Curve-Fit Functions

The coordinates from all the ethylene/air simulations were taken within ANSYS Fluent from the top edge of the ethylene flow where the mass fraction measured 0.03. These data points were then entered into Excel to generate fourth-order polynomial curve fit functions. All of the curve fit functions can be seen plotted against one another in Figure 16, and the curve-fit equations can be seen in Table 4. The simulations with lower momentum ratios did not appear to follow trends seen in theory; however, the higher momentum ratio simulations did agree well.

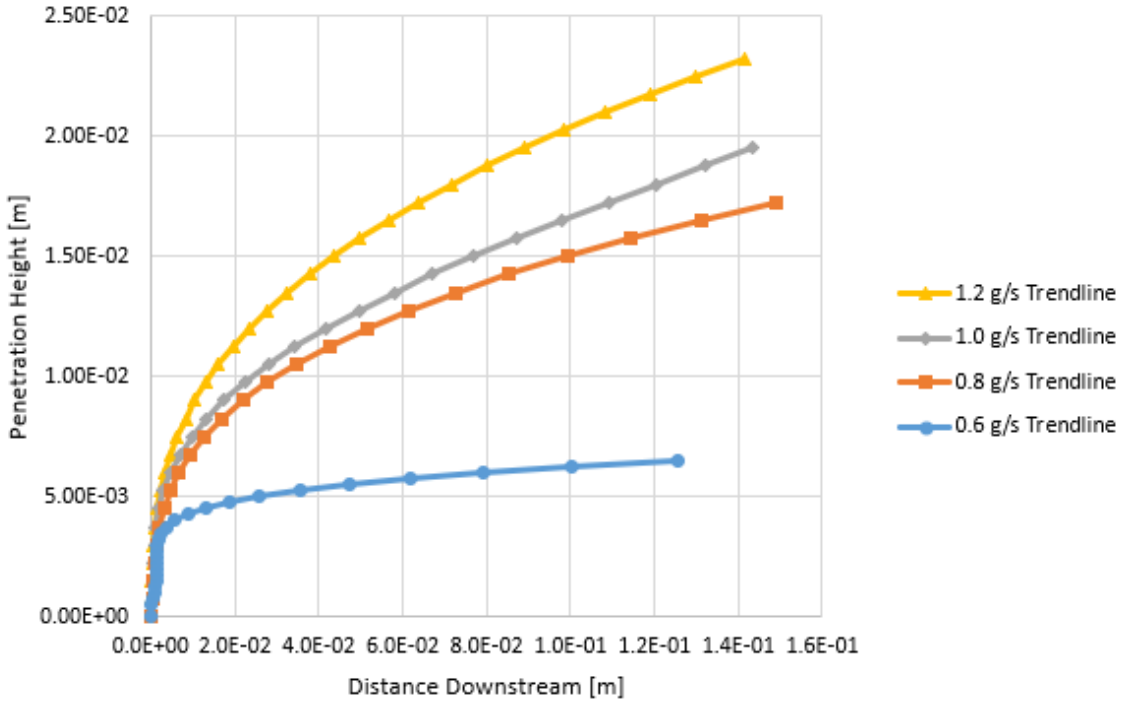

Figure 16. All curve fit functions for the penetration of gaseous ethylene into a crossflow.

Table 4. Ethylene penetration curve fit functions.

C2H4 mass flow rate [g/s]	Curve Fit Function
0.6	$x = (2.500E+08)y^4 - (1.616E+06)y^3 + (3.047E+03)y^2 - (8.705E-01)y$
0.8	$x = (-4.624E+05)y^4 + (4.333E+04)y^3 - (1.387E+02)y^2 + (5.143E-01)y$
1.0	$x = (-1.502E+06)y^4 + (6.166E+04)x^3 - (2.853E+02)x^2 + (6.102E-01)x$
1.2	$x = (-2.167E+05)y^4 + (1.693E+04)y^3 - (2.135E+01)y^2 + (1.504E-01)y$

B. VOF-DPM SIMULATION RESULTS

All VOF-DPM simulations of a single liquid jet into a crossflow were able to be successfully run to the point where each was deemed to have closely approached or have

reached a steady-state solution. Using 256 cores on the Hamming supercomputer, each simulation took approximately 14 days to reach steady state. Images were taken from within ANSYS 2021R1 with a side-profile of the simulation results, creating images similar to those from previous experimentation. The images were then inserted into the same MATLAB tool in order to track the edges of the liquid injection and determine penetration depths, and the resulting data points were brought into Excel for plotting and analysis. Figures 17 and 18 show the liquid injection results for the 3.3 g/s case and the 1.7 g/s case, respectively.

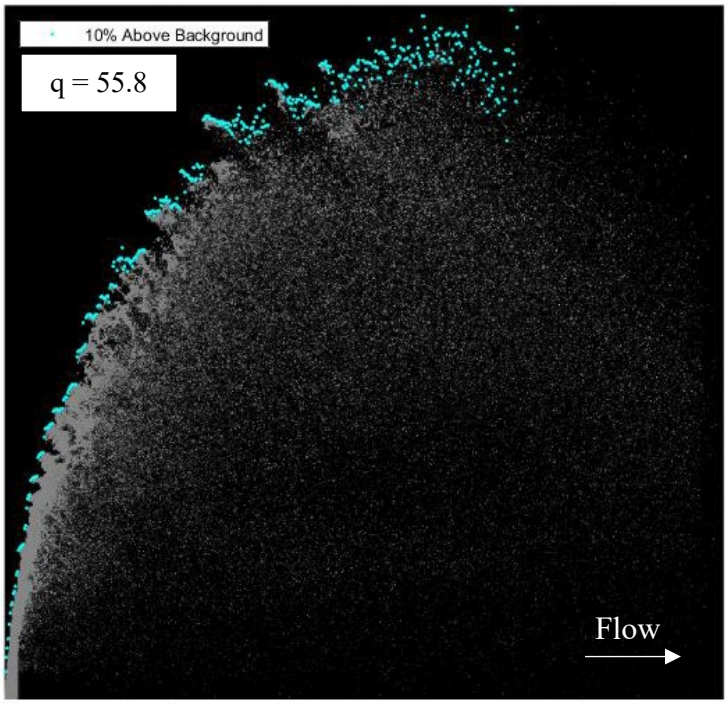

Figure 17. Liquid injection edge detection results for the 3.3 g/s fuel mass flow rate simulation through a 0.381 mm hole.

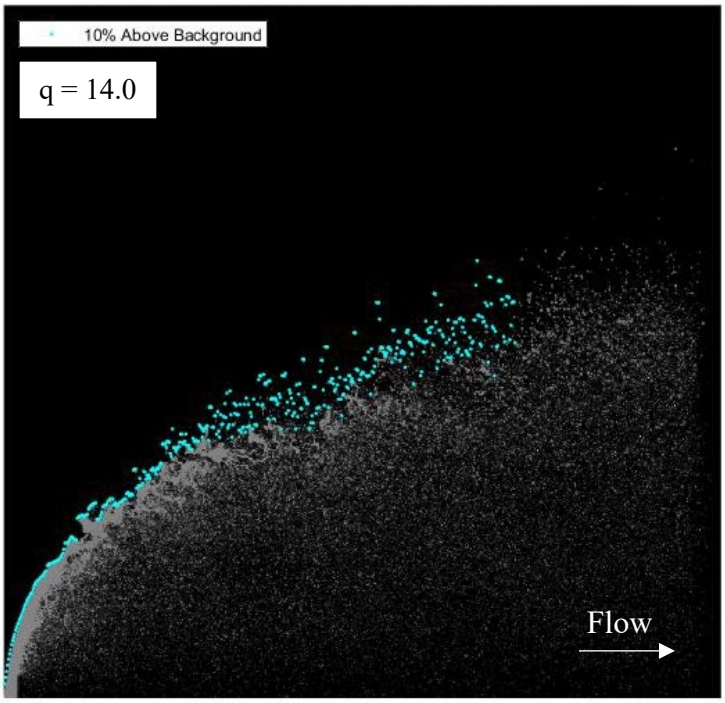

Figure 18. Liquid injection edge detection results for the 1.7 g/s fuel mass flow rate simulation through a 0.381 mm hole.

As anticipated, the 3.3 g/s fuel mass flow simulation results penetrated the test section significantly more than the 1.7 g/s simulation. The higher momentum ratio simulation results also showed that atomization of fuel within the liquid column was further from the injection site, indicating that nearly all of the fuel injected had significant penetration. Large droplets of fuel didn't fully atomize until an approximate downstream location of x/d=20 for the 3.3 g/s simulation.

The 1.7 g/s fuel mass flow rate results in Figure 19 showed much greater atomization closer to the injection site which persisted throughout the fuel's injection. The fuel seemingly split into smaller droplets earlier rather than remain in fewer, larger droplets as in the 3.3 g/s simulation.

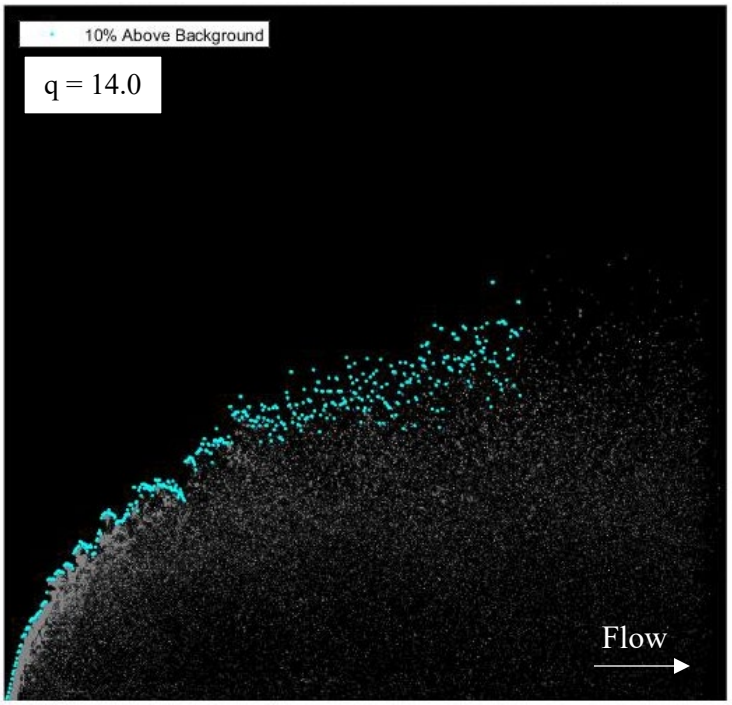

Figure 19. Liquid injection edge detection results for the crescent injector-shape simulation.

The crescent injector-shape results were similar to that of the 1.7 g/s fuel mass flow rate simulation, as seen in Figure 20. The crescent simulation did have slightly lower penetration depth likely due to its lower fuel mass flow rate (0.98 g/s) but had nearly immediate atomization when compared to the 1.7 g/s fuel mass flow case. Immediately after fuel injection, the crescent simulation had visible breakup which continued throughout its penetration of the test volume. The liquid column, as expected, fully broke up much earlier than in the 1.7 g/s flow case, however this can be attributed to the lower fuel mass flow in the simulation allowing a greater influence of the crossflow on the fuel stream.

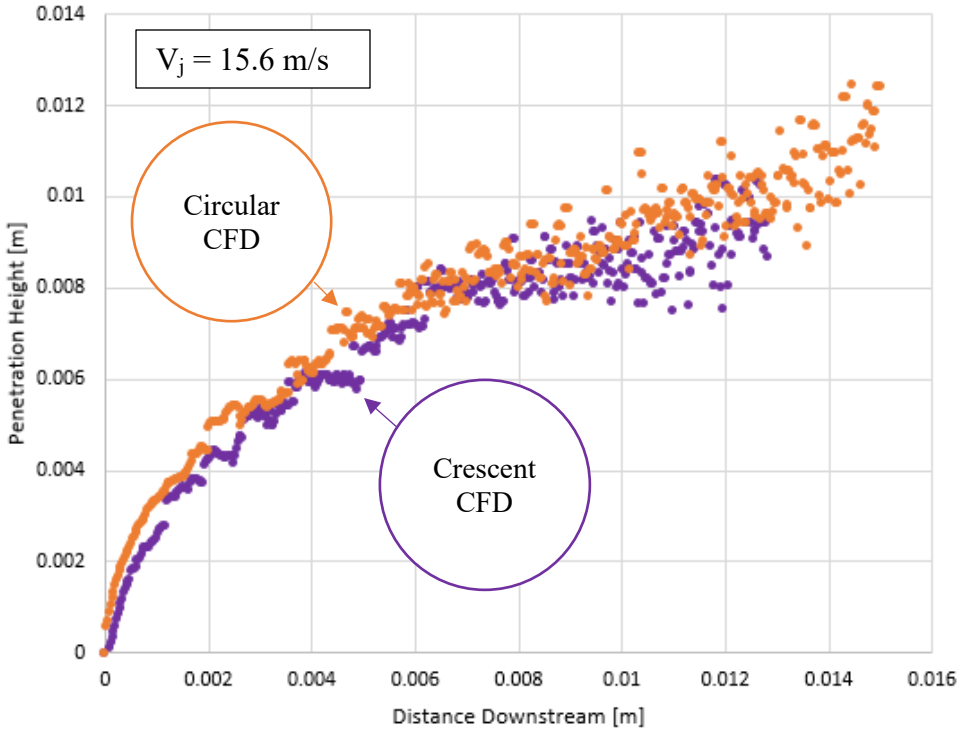

Figure 20. Penetration comparison between the 1.67 g/s fuel mass flow rate simulation and the crescent-shaped injector simulation

C. EXPERIMENTAL IMAGING RESULTS

The sheet lighting of the centerline orifice plane, which Figure 21 shows for multiple trials, yielded insightful images on jet penetration. Determining a luminosity value in the high-speed video that determined if fuel was present proved very challenging for a number of reasons. As the fuel-dye mixture atomized to extremely small droplets, the local droplet density, which is directly proportional to fluorescence signal intensity, would decrease and result in a reduction in fluorescence intensity below the camera detection limits. Additionally, each injection block had multiple injection sites, but the laser sheet only focused on one. The light emitted from excited dye likely reflected and refracted within a single jet's spray as well as through the surrounding jet sprays, obscuring the final video images. A definitive value that indicated the presence of properly atomized fuel within experimental images was not determined, so subjective values of 5% and 10% above the background of each trial's experimental video were chosen. The penetration depth within a single test could also vary both in penetration and luminosity due to slight changes

in the instantaneous fuel mass flow, laser sheet light intensity, and dye concentration, so frames were selected from each trial that best represented the average fuel injection penetration trends.

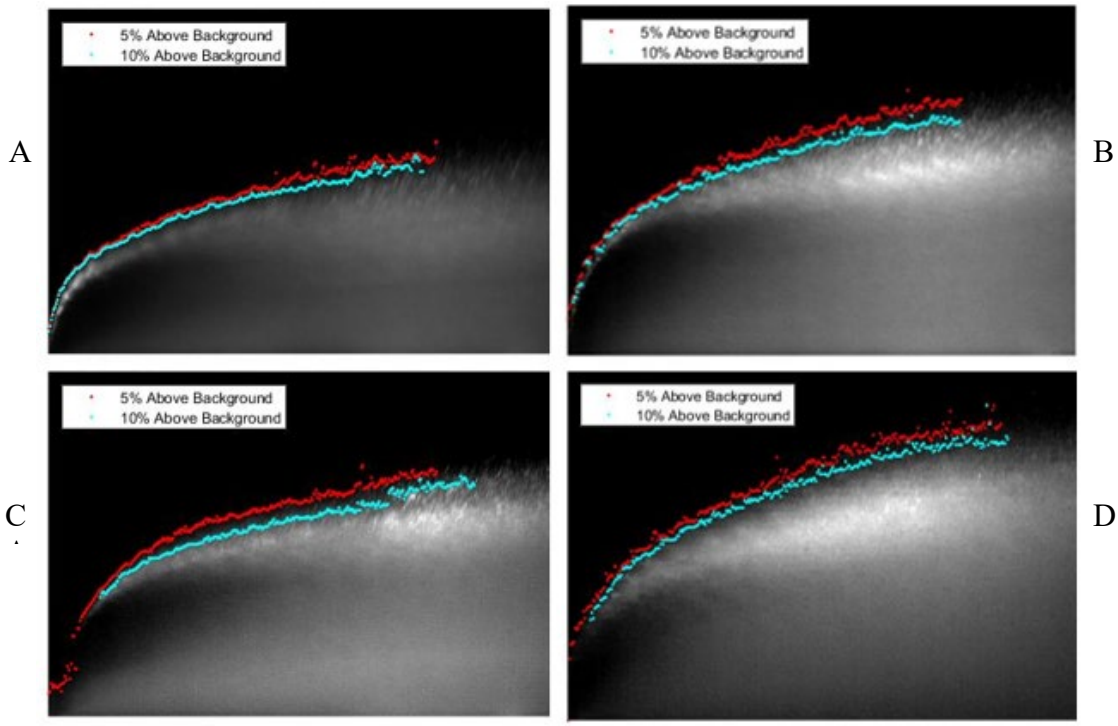

Figure 21. Edge detection results for 0.381mm injector hole sizes made with EDM (A) at 52.0 g/s, additive manufacturing (B) at 49.6 g/s, laser drilling (C) at 47.6 g/s, and platelet design (D) at 42.8 g/s.

Injector blocks of the same design hole size and of different manufacturing methods did not produce similar fuel penetration depths for comparable conditions, as can be seen in Figure 22. Individual 0.381mm injector block results at different fuel mass flow rates can be seen plotted against each other in Appendix C.

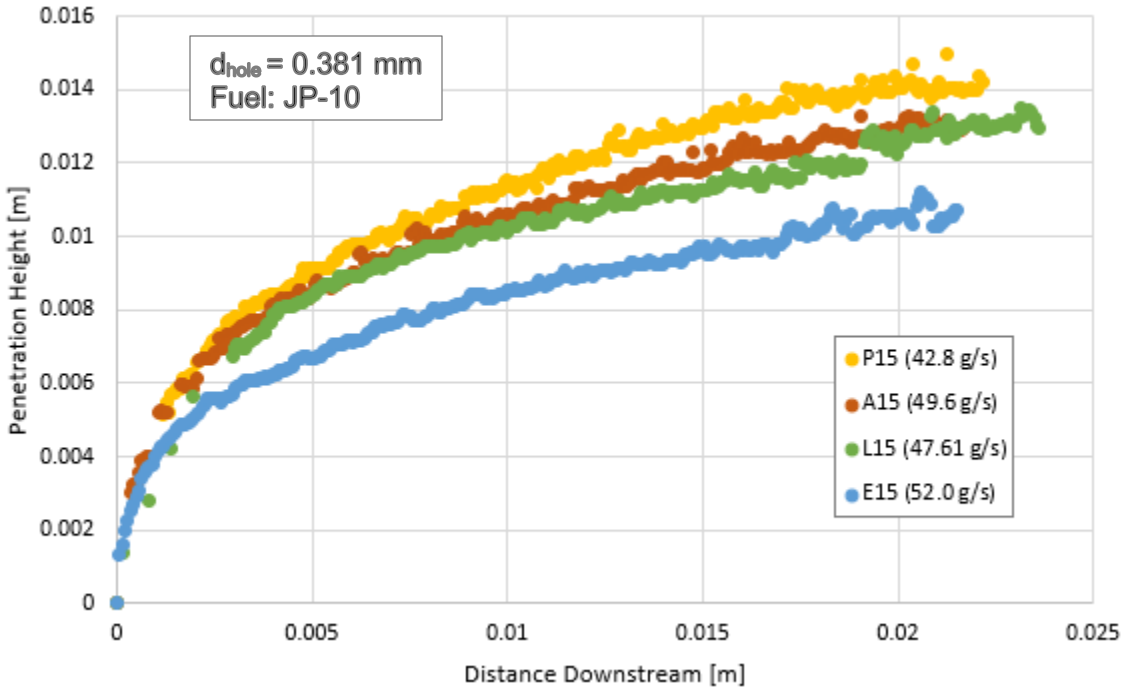

Figure 22. Experimental penetration results for four 0.381mm injector hole sized blocks at similar fuel mass flow rates.

D. VOF-DPM COMPARISON TO EXPERIMENTAL IMAGES

Although the VOF-DPM simulations were able to be ran successfully, some discrepancies were seen between their results and those seen in experimental images. The higher fuel mass flow rate simulation injected noticeably farther than experimental penetration with the same sized injector holes. The simulation assumed that the injection channel was perfectly smooth and circular throughout, which cannot be achieved through all manufacturing methods tested in this thesis. The fuel entrance irregularities within the experimental injector blocks affected the turbulence within the fuel port prior to its injection and likely also influenced the onset of instabilities at the point of injection, resulting in earlier breakup and less penetration of the fuel spray.

The simulations ran in ANSYS Fluent also modeled only a single jet as compared to the 12 jets used in experimental tests which may also explain the difference in results between the two. The simulated crossflow easily flowed around the single jet of liquid fuel as the jet was the only obstruction in the test section volume, whereas the experimental

crossflow encountered a more resistive "wall" of jet fuel due to the linear array of injection sites. The experimental crossflow was then forced to pass over and between the liquid jets, likely exerting a lateral force on the jet fuel, reducing the penetration distance, and increasing its atomization. The blockage effect was seen to be exaggerated at higher flow rates, where the momentum ratio between the fuel and air was higher. The difference between the computational results of the single fuel jet and the experimental image of 12 jets was observed to be the greatest for the high fuel flow rate condition near 3.3 g/s and is depicted in Figure 23.

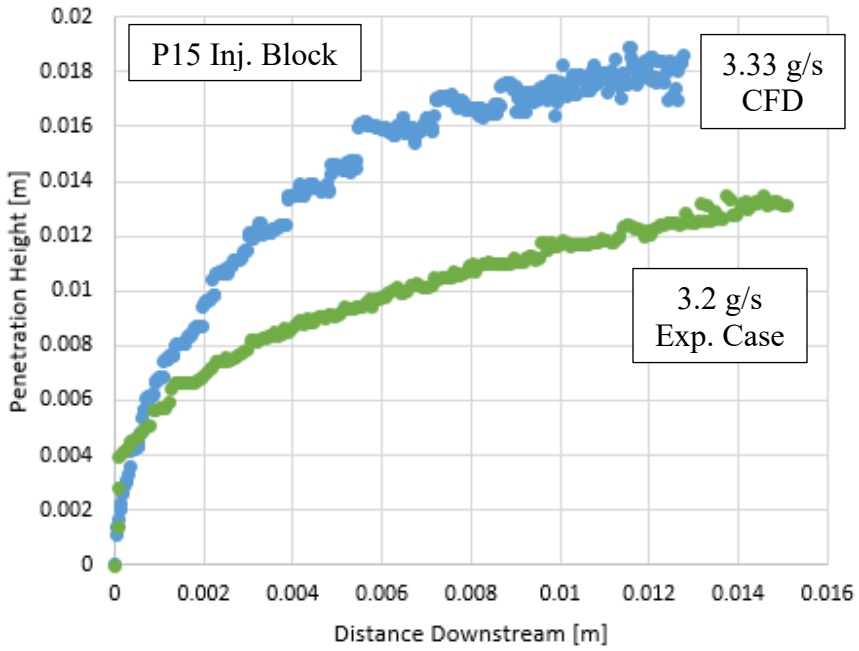

Figure 23. Penetration comparison between a 3.33 g/s fuel mass flow simulation and a 3.2 g/s fuel mass flow experimental result.

The lower mass flow rate simulation correlated more closely to the experimental results, as seen in Figure 24. Although the closest fuel mass flow rate seen in experimental trials was 0.5 g/s higher than the simulated case, the simulated penetration shape closely matches that of the experimental trial. If the simulated mass flow rate was increased to match the experimental trial, the two would have likely followed a very similar penetration path.

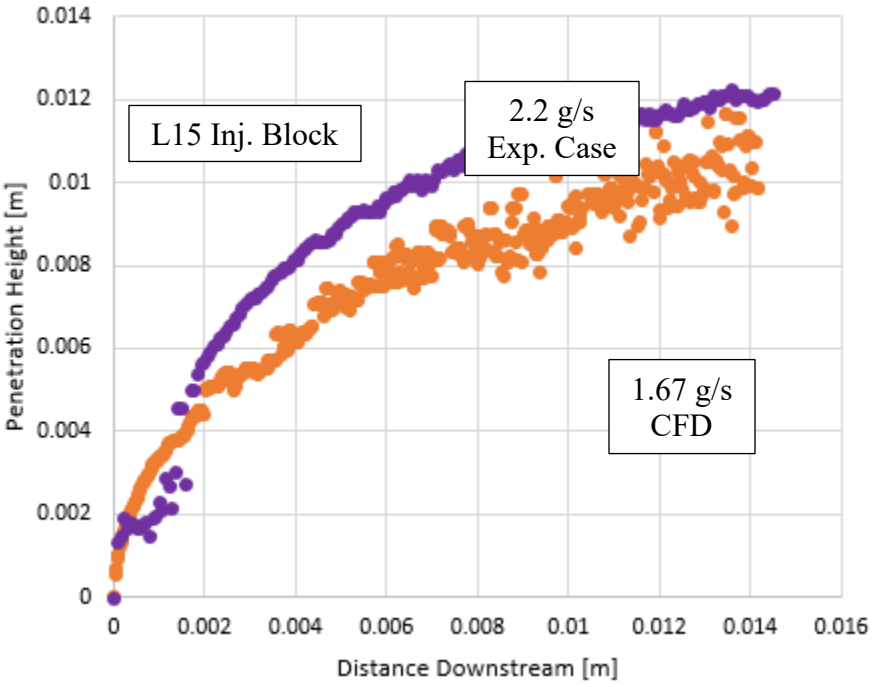

Figure 24. Penetration comparison between a 1.67 g/s fuel mass flow simulation and a 2.2 g/s fuel mass flow experimental result.

VI. SUMMARY AND CONCLUSIONS

Simulations were performed for both ethylene and JP-10 injection into a gaseous crossflow in order to determine how penetration depths compared to analytical solutions and similar experimental conditions.

The gaseous simulations were able to replicate predictions from gas dynamic theory for the higher flow rate conditions but results for the lower momentum simulations revealed Kelvin-Helmholtz instabilities due to the very low fuel injection rates which resulted in deviation from theoretical predictions. The VOF-DPM simulations of JP-10 into a crossflow proved to be capable of handling specified fuel properties and geometry effects. However, spatial dispersion of fuel particles in the simulation volume resulted in challenges for determining local fuel mass fractions due to the discrete particle distribution in the two-phase flow. A method of determining the fuel mass fraction within the air, such as spatial averaging, would aid in determining where proper ignition conditions exist and could improve the characterization of fuel penetration depth and atomization following injection.

The overprediction of jet penetration with VOF-DPM results revealed limitations with modeling a single jet with perfect geometry features. The influence of neighboring jets was observed to reduce jet penetration due to increased crossflow blockage, thereby reducing the effective fuel-air momentum ratio. To accurately model the penetration of an array of liquid fuel injection ports, neighboring injection sites need to be modeled to capture the three-dimensional flow field effects. Additionally, fuel port geometry features such as wall roughness and port interfaces should be accounted for due to their impact on the flow turbulence, velocity profiles, and resulting jet breakup instabilities. Results to date indicate that unique features associated with each fabrication method need to be accounted for in order to obtain higher fidelity simulations of fuel injection and atomization characteristics.

Future fuel injection imaging studies need to include a lateral scan across all fuel jets. This could reveal local fuel-air momentum ratio effects on penetration distance and could shed light on the atomization and breakup between individual liquid jets.

APPENDIX A. INJECTION PLATE IMAGES

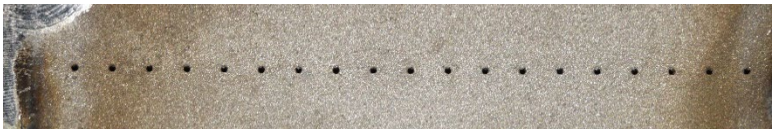

A12 Block (x19)

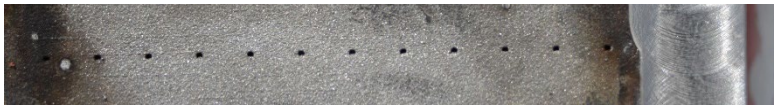

A15 Block (x12)

A20 Block (x7)

A30 Block (x3)

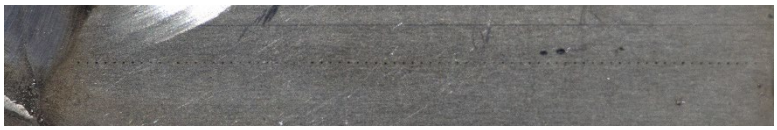

E6 Block (x76)

E8 Block (x42)

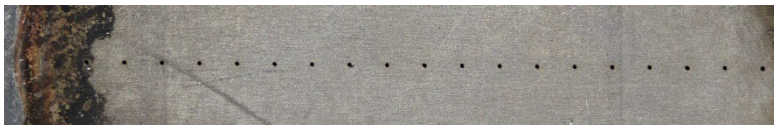

E12 Block (x19)

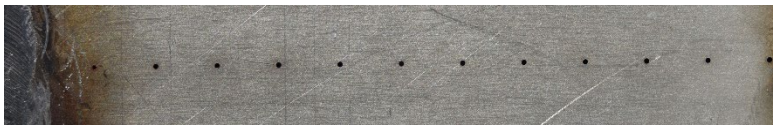

E15 Block (x12)

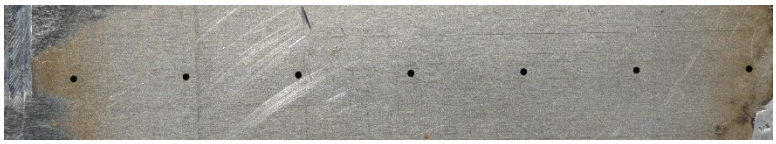

E20 Block (x7)

E25 Block (x4)

L8 Block (x42)

L15 Block (x12)

L20 Block (x7)

APPENDIX B. IMAGE ANALYSIS PROGRAM

```
% ENS Brendan Philbin
% May 2021
% Fuel Injection Curve-Mapping

clear, clear clc, clear figures, format compact

%% CREATE AVERAGE IMAGE

folder = 'C:\Users\2020\Desktop\THESIS\MATLAB Code';

% Load the video
vid = VideoReader('May06Run18x10.avi');

% Set the stop time; this default will just set the stop time as the
end of
% the video file. You can change it to any second-value, i.e. 2 seconds
if
% you only want to loop through part of the video.
stop_time = vid.Duration;

% Set the initial time to begin playback in seconds. A value of 0
% corresponds to the very first frame in the video.
start_time = 0;

% set what frame to start & stop at
% stop_frame = vid.NumFrames;
stop_frame = 300;
start_frame = 1;

% Convert the "start frame" to the appropriate video timestamp and go
to
% that time location within the video
vid.CurrentTime = (start_frame - 1) .* 1/vid.FrameRate

im_avg = zeros(vid.Width,vid.Height);

AllPolys = zeros(300,5);
PolyEdges = zeros(300,301);

% origin = [255,706];  % Pixel location within full sized images (LIQ
INJ)
origin = [281,792];
% origin = [332,756];

% for ii = start_frame:1:stop_frame
for ii = start_frame:1:vid.NumFrames
   % read the current frame
   current_frame = im2gray(readFrame(vid));
```

```
    % convert the frame from a uint8 value to an intensity scale from 0-
1
    current_frame = double(current_frame) ./ 255;
    % Add the frames to take an average later
    im_avg = im_avg + current_frame;
    % Save one (randomly picked) frame for analyzing individually
    if ii == 151
        savedframe = current_frame;
    end
end

% Average polynomial curves together for an average curve
AvgPoly = mean(AllPolys);

% Average tracked edges together to find average jet-edge path
AvgEdge = mean(PolyEdges);

% Divide the sum total intensity by the total number of frames
im_avg = im_avg ./ (stop_frame - start_frame - 1);
%============== CHANGING TO SINGLE FRAME, NOT AVERAGE IMAGE
================
% videoimage = imread('fullflow_image_color.jpg');
% videoimage_bw = im2gray(videoimage);
% videoimage_bw = double(videoimage_bw) ./ 255;

% im_avg = videoimage_bw;
im_avg = savedframe;
im_avg = imrotate(im_avg',270);

% Normalize image data
im_avgnorm = im_avg/(max(max(im_avg)));

% figure(1)
% imshow(im_avg);
% title('Averaged Image')

figure(1)
imshow(im_avgnorm);
title('Normalized Average Image')


%% Calibration Image Processing

% Calibration image is "RigCalibration_2020.tif"
tif = Tiff('RigCalibration_2020.tif','r');
CalibrationImage = read(tif);
% figure(2)
% imshow(CalibrationImage)

% TOP EDGE OF RULER
% Point 1 is at [94 323]
% Point 2 is at [455 333]
% Distance between two points is one inch
```

```
% Equates to 361.1385 pixels per inch; 0.002769 in per pixel
% Equates to 142.1805 pixels per cm; 0.007033 cm per pixel

% BOTTOM EDGE OF RULER
% Point 1 is at [84 679]
% Point 2 is at [445 688]
% Distance between two points is one inch
% Equates to 361.1122 pixels per inch; 0.002769 in per pixel
% Equates to 142.1701 pixels per cm; 0.007034 cm per pixel

% === AVERAGE ===
% Standard: 361.1253 pixels per inch; 0.002769 in per pixel
% Metric: 142.1753 pixels per cm; 0.007034 cm per pixel


%% METHOD: Tracing the edge of the jet

% Create binary map
sensitivity = 0.10;  %***THIS is what will control the sensitivity of
the
                  % binary map. The higher the number, the brighter the
                  % original image must be to be "noticed"
binaryImage = im_avg > sensitivity;

% Flip image data and plot
grayflip = abs(binaryImage - 1);

% Get initial binary location data
[rows, columns] = find(binaryImage); % Finds locations of all dark
points
[a,b] = size(binaryImage); % Sizes image
edgedata = zeros([size(columns,1),2]);
rows = (a+1) - rows; % Mirrors row values so that resulting collected
data
                    % points are able to properly be plotted in Fig 2

% Detect location of edge
for i = 1:(length(columns)-1)
   if columns(i+1) - columns(i) == 1
       edgedata(i+1,1) = rows(i+1);
       edgedata(i+1,2) = columns(i+1);
   end
end

% Remove zeros from edge data
edge_rows = nonzeros(edgedata(:,1));
edge_cols = nonzeros(edgedata(:,2));
edgepts = [edge_rows edge_cols];

% Designate jetstream origin  ***Must be located MANUALLY***
% origin = [332,756];  % Pixel location within full sized images
origin = [((a-1)-origin(2)) origin(1)];  % Readjust for
plotting/analysis
```

```
% origin = [((a-1)-757) 338];  % Entered [y, x], this one's at 338,757
edgepts = [origin; edgepts]; % Insert origin into edge data

% Correct jetstream points so that they are centered at (0,0)
edgeplot = [(edgepts(:,1)-origin(1))  (edgepts(:,2)-origin(2))];

% Calculate polynomial to fit edge points
p = polyfix(edgeplot(:,2),edgeplot(:,1),4,0,0);
   % If p = [1 2 3], the polynomial is  x^2 + 2x + 3

x = [0:300];
y = polyval(p,x);


%% METHOD: Removing 5% noise

im_5prem = zeros(a);
for j = 1:a
   for jj = origin(2):(origin(2) + 310)  % takes 310 columns downstream
of origin
       if im_avgnorm(j,jj) < 0.05   % Defines percent removal
           im_5prem(j,jj) = 0;
       else
           im_5prem(j,jj) = im_avgnorm(j,jj);
       end
   end
end

% Get initial binary location data
[rows_5pr, columns_5pr] = find(im_5prem); % Finds locations of all dark
points
edgedata_5pr = zeros([size(columns_5pr,1),2]);
rows_5pr = (a+1) - rows_5pr; % Mirrors row values so that resulting
collected data
                    % points are able to properly be plotted in Figure

% Detect location of edge
for i = 1:(length(columns_5pr)-1)
   if columns_5pr(i+1) - columns_5pr(i) == 1
       edgedata_5pr(i+1,1) = rows_5pr(i+1);
       edgedata_5pr(i+1,2) = columns_5pr(i+1);
   end
end

% Remove zeros from edge data
edge_rows_5pr = nonzeros(edgedata_5pr(:,1));
edge_cols_5pr = nonzeros(edgedata_5pr(:,2));
edgepts_5pr = [edge_rows_5pr edge_cols_5pr];

% Designate jetstream origin  ***Must be located MANUALLY***
edgepts_5pr = [origin; edgepts_5pr]; % Insert origin into edge data

% Correct jetstream points so that they are centered at (0,0)
```

```
edgeplot_5pr = [(edgepts_5pr(:,1)-origin(1))  (edgepts_5pr(:,2)-
origin(2))];


%% Produce Final Results Plot

% Trim im_avgnorm for comparison plot below
    % *Origin is put in lower left corner of image
    % *Image is made to be 350x250 pixels (landscape, not portrait)
im_snip = im_avgnorm(:,(origin(2)):(origin(2)+400));
im_snip = im_snip((a-origin(1)-250):(a-origin(1)),:);
[snip_h, snip_l] = size(im_snip);

% % Trim im_avgnorm for comparison plot below FOR LIQUID
INJECTION*********
%      % *Origin is put in lower left corner of image
%      % *Image is made to be 350x250 pixels (landscape, not portrait)
% im_snip = im_avgnorm(:,(origin(2)):(origin(2)+700));
% im_snip = im_snip((a-origin(1)-675):(a-origin(1)),:);
% [snip_h, snip_l] = size(im_snip);

% Plot analysis results over normalized image snip
figure(4)
imshow(im_snip)
hold on
plot(edgeplot_5pr(:,2),snip_h-
edgeplot_5pr(:,1),'.r',edgeplot(1:300,2),snip_h-edgeplot(1:300,1),'.c')
% plot(edgeplot(1:450,2),snip_h-edgeplot(1:450,1),'.c')
axis([0 400 0 250])
title('Image Analysis Results (Background: Normalized Image)')
legend('5% Above Background','10% Above
Background','Location','northwest')
% legend('10% Above Background','Location','northwest')
hold off
```

THIS PAGE INTENTIONALLY LEFT BLANK

APPENDIX C. EXPERIMENTAL VIDEO IMAGING RESULTS

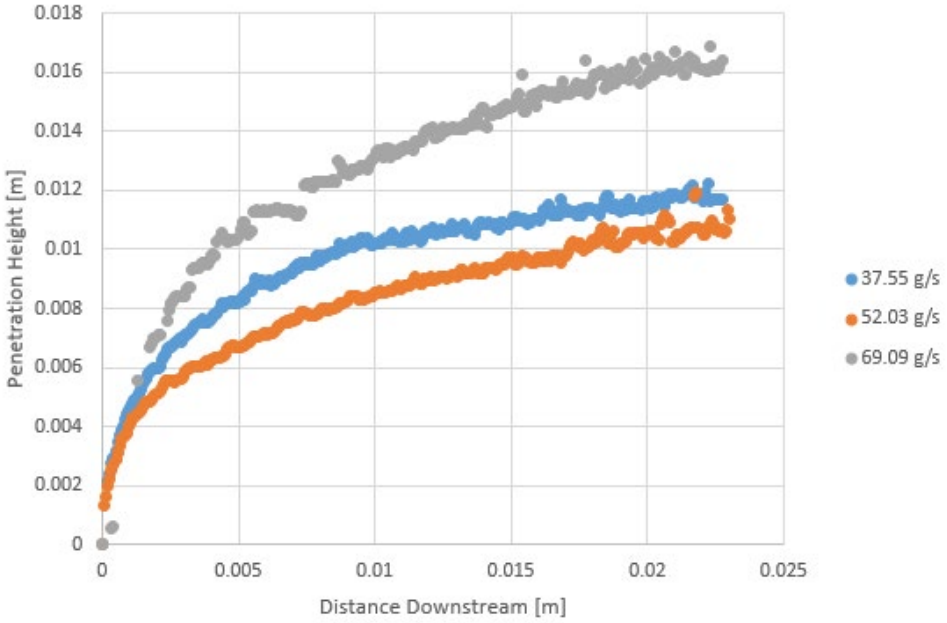

E15 injector block penetration depth results.

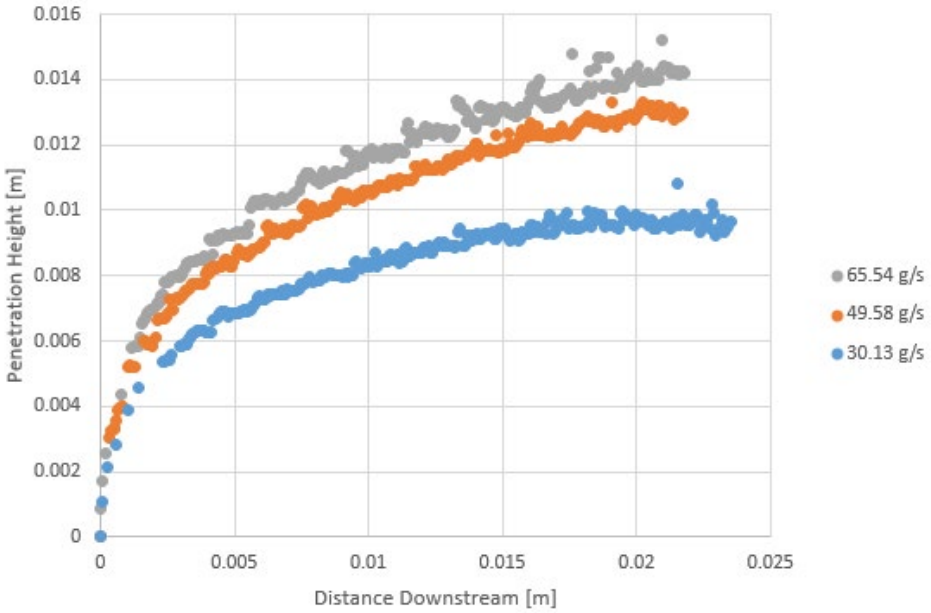

A15 injector block penetration depth results.

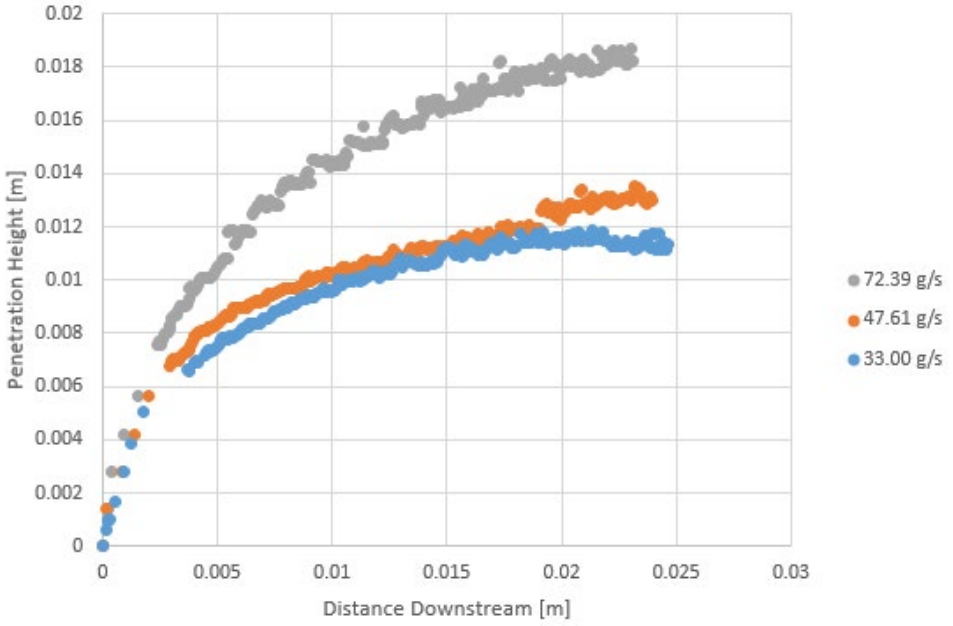

L15 injector block penetration depth results.

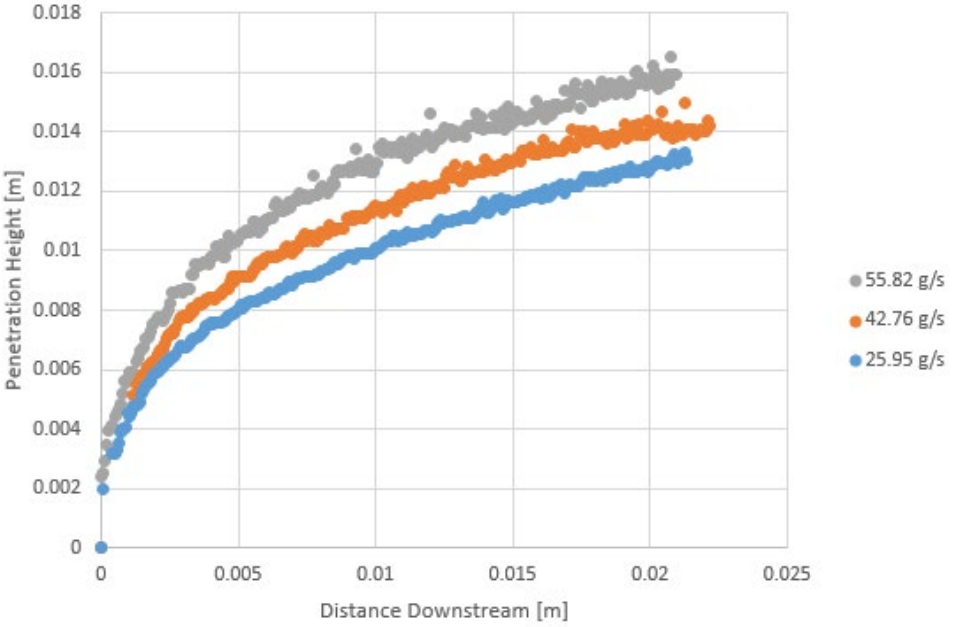

P15 injector block penetration depth results.

LIST OF REFERENCES

[1] A. Lefebvre and V. McDonell. *Atomization and Sprays*. 2nd ed. Boca Raton: CRC Press LLC, 2017.

[2] P. Wu, Kevin A. Kirkendall, and R. P. Fuller. "Breakup processes of liquid jets in subsonic crossflows," *Journal of Propulsion and* Power, vol. 13, no. 1, Jan 1997. [Online] doi: https://doi-org.libproxy.nps.edu/10.2514/2.5151

[3] S.-Y. No, "A review on empirical correlations for jet/spray trajectory of liquid jet in uniform cross flow," *International Journal of Spray and Combustion Dynamics*, vol. 7, no. 4, pp. 283–313, 2015.

[4] M. Marzbali. "Penetration of circular and elliptical liquid jets into gaseous crossflow: A combined theoretical and numerical study," M.S. thesis, Dept. of Mech. and Industrial Eng., Concordia Univ., Montreal, Quebec Canada, 2011.

[5] C. Tam, S. Cox-Stouffer, K. Lin, K., M. Gruber and T. Jackson, "Gaseous and liquid injection into high-speed crossflows," *43rd AIAA Aerospace Sciences Meeting and Exhibit*, Jan 2005. [Online]. doi: https://doi.org/10.2514/6.2005-301

[6] J. N. Stenzler, J. G. Lee, and Domenic A. Santavicca. "Penetration of liquid jets in a crossflow," *41st Aerospace Sciences Meeting and Exhibit*, Jan 2003. [Online]. doi: https://doi-org.libproxy.nps.edu/10.2514/6.2003-1327

[7] D. Hautman, R. Haas, and L. Chiappetta. "Transverse gaseous injection into subsonic air flows," *29th Aerospace Sciences Meeting*, Jan 1991. [Online] doi: https://doi-org.libproxy.nps.edu/10.2514/6.1991-576

[8] M. Broumand and M. Birouk. "Two-zone model for predicting the trajectory of liquid jet in gaseous crossflow," *American Institute of Aeronautics and Astronautics*, vol. 54, no. 5, May 2016. [Online] doi: https://doi-org.libproxy.nps.edu/10.2514/1.J054440

[9] S. Tmabe, S. Jeng, H. Mongia, and G. Hsiao. "Liquid jets in subsonic crossflow," *43rd AIAA Aerospace Sciences Meeting and Exhibit*, Jan 2005. [Online] doi: https://doi-org.libproxy.nps.edu/10.2514/6.2005-731

[10] K.-C. Lin, P. Kennedy, and T. Jackson. "Spray structures of aerated-liquid jets in subsonic crossflows," *39th Aerospace Sciences Meeting and Exhibit*, Jan 2001. [Online] doi: https://doi-org.libproxy.nps.edu/10.2514/6.2001-330

THIS PAGE INTENTIONALLY LEFT BLANK

INITIAL DISTRIBUTION LIST

1. Defense Technical Information Center
   Ft. Belvoir, Virginia

2. Dudley Knox Library
   Naval Postgraduate School
   Monterey, California